fibers

Tracked for Impact Factor

CITESCORE 6.5

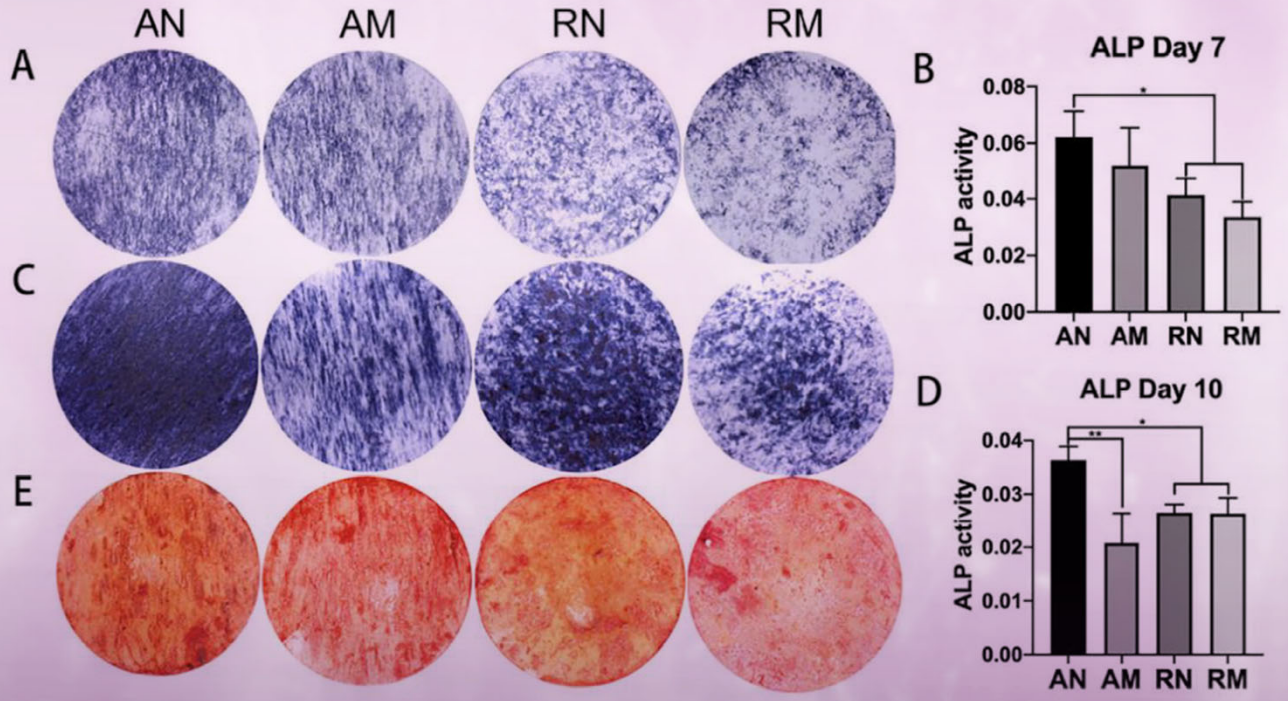

Physical Properties of Fiber Scaffolds Affecting Tissue Engineering Outcomes

Volume 11 · Issue 5 | May 2023

MDPI

mdpi.com/journal/fibers
ISSN 2079-6439

fibers

MDPI

Review

Mechanical Properties and Morphological Alterations in Fiber-Based Scaffolds Affecting Tissue Engineering Outcomes

James Dolgin [1,2], Samerender Nagam Hanumantharao [3], Stephen Farias [1,2], Carl G. Simon, Jr. [4] and Smitha Rao [3,5,6,7,*]

1 Materic LLC, 1100 Wicomico St. Ste. 323, Baltimore, MD 21230, USA; stephen.farias@dipolematerials.com (S.F.)
2 Dipole Materials Inc., 1100 Wicomico St. Ste. 323, Baltimore, MD 21230, USA
3 Department of Biomedical Engineering, Michigan Technological University, 1400 Townsend Dr., Houghton, MI 49931, USA; samerendernh@gmail.com
4 National Institute of Standards and Technology (NIST), 100 Bureau Drive, Gaithersburg, MD 20899, USA; carl.simon@nist.gov
5 Great Lakes Research Center, Michigan Technological University, 1400 Townsend Dr., Houghton, MI 49931, USA
6 Health Research Institute, Michigan Technological University, 1400 Townsend Dr., Houghton, MI 49931, USA
7 Department of Biological Sciences, Michigan Technological University, 1400 Townsend Dr., Houghton, MI 49931, USA
* Correspondence: smithar@mtu.edu

Abstract: Electrospinning is a versatile tool used to produce highly customizable nonwoven nanofiber mats of various fiber diameters, pore sizes, and alignment. It is possible to create electrospun mats from synthetic polymers, biobased polymers, and combinations thereof. The post-processing of the end products can occur in many ways, such as cross-linking, enzyme linking, and thermal curing, to achieve enhanced chemical and physical properties. Such multi-factor tunability is very promising in applications such as tissue engineering, 3D organs/organoids, and cell differentiation. While the established methods involve the use of soluble small molecules, growth factors, stereolithography, and micro-patterning, electrospinning involves an inexpensive, labor un-intensive, and highly scalable approach to using environmental cues, to promote and guide cell proliferation, migration, and differentiation. By influencing cell morphology, mechanosensing, and intracellular communication, nanofibers can affect the fate of cells in a multitude of ways. Ultimately, nanofibers may have the potential to precisely form whole organs for tissue engineering, regenerative medicine, and cellular agriculture, as well as to create in vitro microenvironments. In this review, the focus will be on the mechanical and physical characteristics such as porosity, fiber diameter, crystallinity, mechanical strength, alignment, and topography of the nanofiber scaffolds, and the impact on cell proliferation, migration, and differentiation.

Keywords: tissue engineering; scaffolds; mechanotransduction; biophysical cues; electrospinning

Citation: Dolgin, J.; Hanumantharao, S.N.; Farias, S.; Simon, C.G., Jr.; Rao, S. Mechanical Properties and Morphological Alterations in Fiber-Based Scaffolds Affecting Tissue Engineering Outcomes. *Fibers* **2023**, *11*, 39. https://doi.org/10.3390/fib11050039

Academic Editor: Natalia Mihailescu

Received: 13 March 2023
Revised: 18 April 2023
Accepted: 25 April 2023
Published: 29 April 2023

1. Introduction

1.1. Nanofiber Scaffolds in Tissue Engineering

Scaffolds are an important part of the grand challenge of creating whole organs in the field of tissue engineering and regenerative medicine. Mechanotransduction is a powerful tool for initiating and maintaining intercellular events, including cascades of protein signaling, which can lead to adhesion, propagation, and differentiation. Mechanical cues have been shown to be 40 times faster than biochemical cues in inducing signaling in some cases [1]. While micropatterning and other microfabrication techniques [2,3] can recapitulate the intricately structured microenvironment of native tissue, these fabrication techniques lack the scalability and cost effectiveness of electrospinning. More recently, there has been interest in mass production. Furthermore, there is an ever-pressing need for realistic models for in vitro analysis and in vivo applications. In all these applications, there

is an inherent need to understand the relationships that exist between scaffold properties and cells. The ability to tune these properties appears to be the key to establishing 3D cell cultures, organ-on-chip, organoids, and in vitro models. As an example, a scaffold made from poly(lactic-co-glycolic acid) for primary human bone marrow stromal cell is shown in Figure 1. Poly(lactic-co-glycolic acid) nanofibers obtained from electrospinning were used as a substrate to culture primary human bone marrow stromal cells. As seen in Figure 1, the nanofibers promote the adhesion, elongation, and infiltration of the cells into the nanofibers by providing a 3D environment for the cells.

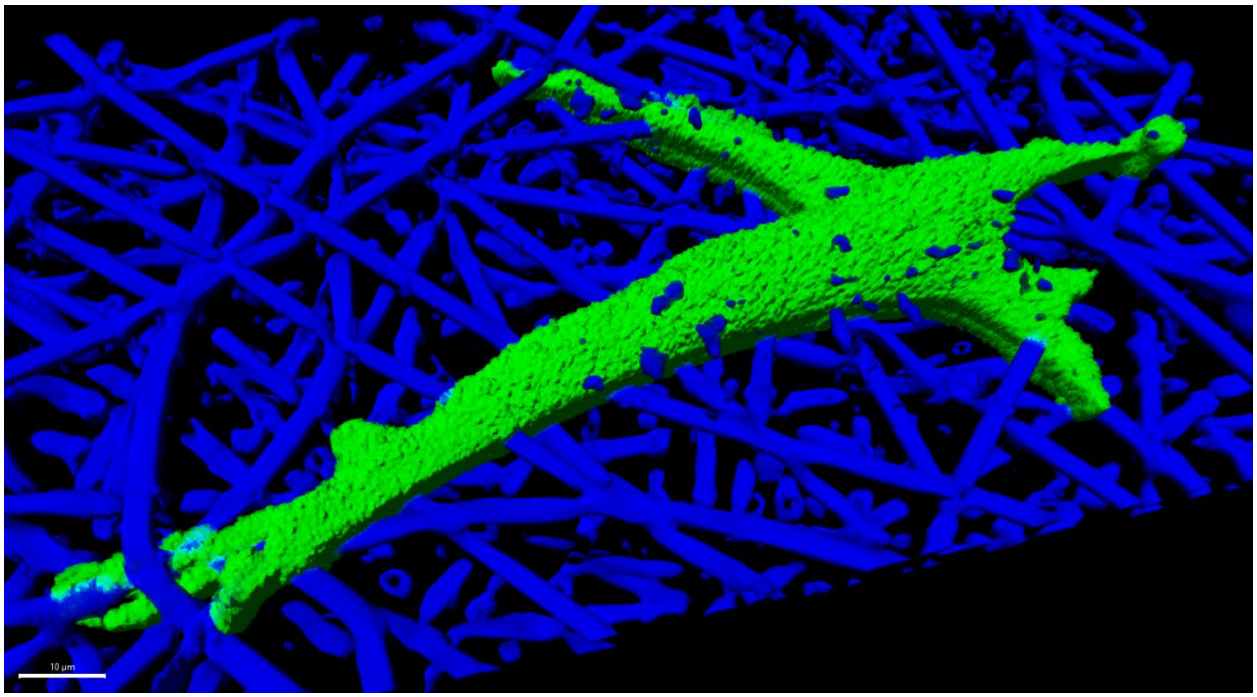

Figure 1. Primary human bone marrow stromal cells cultured 24 h in an electrospun fiber scaffold made of poly(lactic-co-glycolic acid), with a nominal fiber diameter of 2.7 µm. The 3D rendering was created from z-stacks captured by confocal fluorescence microscopy using a cell channel (OregonGreen-Maleimide 488) and a scaffold channel (Flamma Fluor FKR648). The fibers were rendered fluorescent by spiking fluor into the polymer solution prior to electrospinning. Image Credit: Carl Simon, NIST.

The extracellular matrix (ECM) is known to play a key role in tissue homeostasis and function. For example, the mechanical regulation of ECM stiffness plays an important role in cell growth, differentiation, and migration [4–8]. Much work has focused on presenting the biochemical environment surrounding the extracellular matrix around different organ systems, or replicating the biomechanical features of the ECM as experienced by the cells [9]. Natural and synthetic materials have been explored and different techniques to establish the ECM, such as patterned substrates, hydrogels, soft biopolymers, and nanofibers, have been reported [10–13]. Nanofiber scaffolds are characterized according to the mechanical properties of the fibers, pore size, crystallinity, and fiber alignment and morphology. Each one of these attributes, by itself or in combination, uniquely impacts cell adhesion, alignment, proliferation, and differentiation. For example, the elasticity and stiffness of the substrate have been reported to impact cell migration [7,8,14]. This is attributed to "Durotaxis", or the response to mechanical stiffness, and refers to the preferential migration observed in cells cultured on stiffer substrates, as compared to less rigid or softer substrates.

In addition, in nanofibers, other parameters can be manipulated that directly affect cell adhesion and proliferation. Porosity is a measurement of the percent of open space in

electrospun mats, and pore size is the average diameter of these open spaces [15]. Pore size can be controlled through various electrospinning parameters and post-processing steps, though there is conflicting research regarding the influence of fiber size on pore size [16,17]. Pore sizes can range from nanometers to a few millimeters. While nanoscale pores have been shown to impact the formation of collagen and ECM [18], cell density, migration, and vascularization are impacted by macroscale pores [19–21]. Furthermore, cell migration is reported to be linearly dependent on pore size [22]. Microenvironmental properties are crucial to determine the fate of mesenchymal stem cells (MSCs). It has been shown that simple alterations in the pore size of honeycomb scaffolds can change the fate of MSCs of forming myogenic or osteogenic cells, based on osteopontin and MyoD1 staining [23]. Thus, the ability to control stiffness, porosity, and pore size has a direct impact on tissue engineering and potential applications in regenerative medicine [24].

Nanofiber alignment not only significantly impacts the mechanical properties of meshes [25], but also has a direct effect on actin alignment in MSCs [26]. Many studies have shown that the fiber orientation of the substratum influences cell adhesion and growth, [27–29], and modulates the elongated cellular patterns that are typical of native tissues [30,31]. Nanofiber scaffolds with a topography such as native tissue have the ability to direct the alignment of cells and subcellular structures, and successively allow for the deposition of collagen along the electrospun nanofiber direction that will result in an increase in the tensile properties of the new tissue [32]. Aligned nanofiber scaffolds exhibited a higher modulus than the random nanofibers in a study reported by Pauly et al. (2016) [9]. They also reported scaffolds with mechanical properties (modulus, yield stress, and yield strain) within the range of native tissues. Similarly, in the muscles, the muscle fibers are aligned along an axis and are formed by a single cell [33]. This uniaxial alignment is the key in developing engineered muscle tissues. Such physiologically relevant models could prove to be a suitable alternative to animal models for drug testing.

In addition to alignment, the fiber diameter directly impacts the mechanical strength of the nanofiber scaffolds and affects the growth of various tissues. The mechanical properties of the nanofiber scaffolds can therefore be tuned by either manipulating the alignment, fiber morphology, or a combination of the features. Similarly, changes in crystallinity impact mechanical properties of nanofibers, which dictates the outcomes for differentiation. The swelling of the fibers and the degree of crystallinity, in turn, affects the behavior of cells seeded on the scaffold. Thus, the properties can be tuned to influence outcomes such as the differentiation of either muscle [34,35] or bone [36,37] tissues through the modulation of mechanical properties. It has also been shown that myogenic differentiation typically prefers increases in elasticity over the enhancement of crystallinity [38,39], while osteogenic differentiation is greatly enhanced by crystallinity increases, despite drastic reductions in elasticity and strength [40,41].

Three-dimensional nanofiber-based in vitro systems could be more affordable and effective than animal models which are often costly, labor intensive, and potentially ethically controversial [42]. Hence, creating platforms that accurately recapitulate the tissue environment for precise regenerative applications is of pressing importance.

Many techniques have been advanced for fabricating fiber scaffolds, including, but not limited to, the following: electrospinning, forcespinning [43], meltspinning [44], pneumatospinning [45], blowspinning [46], melt-electrowriting [47], melt extrusion [48], wet extrusion [49], fused deposition [50], liquid crystal deposition [51], electrochemical alignment [52], drawing [53], spinning, knitting [54], weaving [55], braiding [56], powder bed fusion (laser sintering), vat photopolymerization (stereolithography) [57], binder jetting [58], directed energy deposition [59], self-assembly (for example, fibrillogenesis) [60], and hybrid approaches [15]. Although electrospun fibers are the primary focus, this article has bearing on fibers made via any of these methods.

Although the characterization of fiber constructs is important, this topic is not covered in the current review. The reader may refer to the FDA guidance on surgical meshes [61],

the ASTM standard guide for characterizing fiber-based constructs [15], and a recent review [62] for further information of this specific topic.

1.2. Electrospinning

Electrospinning is a versatile technique invented in 1931 by Anton Formhals [63], during which electrostatic forces are used to atomize polymer solutions for the fabrication of nanofibers and scaffolds with complex geometries [64–68]. A typical electrospinning setup consists of a power source, a syringe pump connected to a narrow needle via tubing, and a collector (Figure 2). Electrospinning conventionally uses a direct current (direct electrospinning), though alternating current electrospinning has been employed as well for enhanced production [69]. In electrospinning, a voltage bias is applied across the needle and the collector, on the surface of which nanostructures are obtained in the form of nanofibers and nanoparticles, depending on the parameters used for electrospinning. A Taylor cone is created when the electric field is greater than the surface tension of the polymer solution. The charged polymer solution travels to the oppositely charged voltage bias (collector) in the form of a jet. The jet elongates along a linear trajectory and then splits into multiple streams caused by solvent evaporation and divergent electric field forces. The jet flow becomes more turbulent as it approaches the collector, and this chaotic motion is affected by solution properties, collector distance, and voltage. These parameters subsequently affect the crystallinity and lattice structure of the polymeric nanostructures. Other electrospinning parameters, such as collector properties and environmental factors, also dictate nanofiber outcomes [70]. Environmental conditions, namely temperature, humidity and atmospheric pressure, affect the formation of the Taylor cone and resultant nanostructures. This has been used to make unique nanostructures [71–73]. Climate controlled setups are currently being used to improve the reproductivity of the formation of nanostructures. The collector, which can be a solid or liquid surface, can also lead to the formation of unique nanostructures, depending on the type of collector used [74]. To better understand the electrospinning processes and provide the means to theoretically determine the formation of the Taylor cone, properties of the resultant nanostructure and ideal electrospinning conditions, we direct the readers to these excellent references [71–81].

Electrospinning parameters and their outcomes have been studied extensively, and the customization of these outcomes holds great promise for the field of creating diverse tissue engineering nanomaterials. Factors such as electric field, negative electric bias, and alternating voltage have been used to alter the morphology of nanostructures [69,82]. Various collector configurations, including rotating drums, patterned collectors, liquid-containing collectors, parallel electrodes, and magnetically charged electrodes have been used to diversify nanostructure morphology [83–89]. Spinneret modifications, such as coaxial spinnerets, multi-axle spinneret, melt, in-line polymer blending, and co-electrospinning configurations have been used to create complex 3D patterns and multi-material structures [90–92]. The properties of the polymeric solution, including solubility of the polymer in the solvent, polymer flow rate, polymer viscosity, molecular weight of the polymer, boiling point of the solvent, presence of additives, miscibility of the solution and, in certain cases, the magnetic properties of the solution [93,94], contribute to the structure, morphology, porosity and other characteristics of the fibers produced. Sacrificial polymers can also be added to electrospinning solutions, and later dissolve or thermally degrade to create porous or mesoporous structures [95].

A large number of synthetic, natural and mixed polymer blends have been used for electrospinning scaffolds [96–100]. The choice of material used is greatly dependent on the intended application. It is also dependent upon the specific tissue type, although this has not been fully explored. However, an important criterium is to ensure the biocompatibility of the materials used to synthesize the scaffold. Biocompatibility is defined as "the ability of a material to perform with an appropriate host response in a specific application." The review by Ghasemi-Mobarakeh et al., (2019), highlights some of the key concepts and terminology in biomaterial design and biocompatibility [101]. The following sections will

focus on some of the specific mechanical characteristics that are important for engineering tissues, challenges associated with it, and the current research focus.

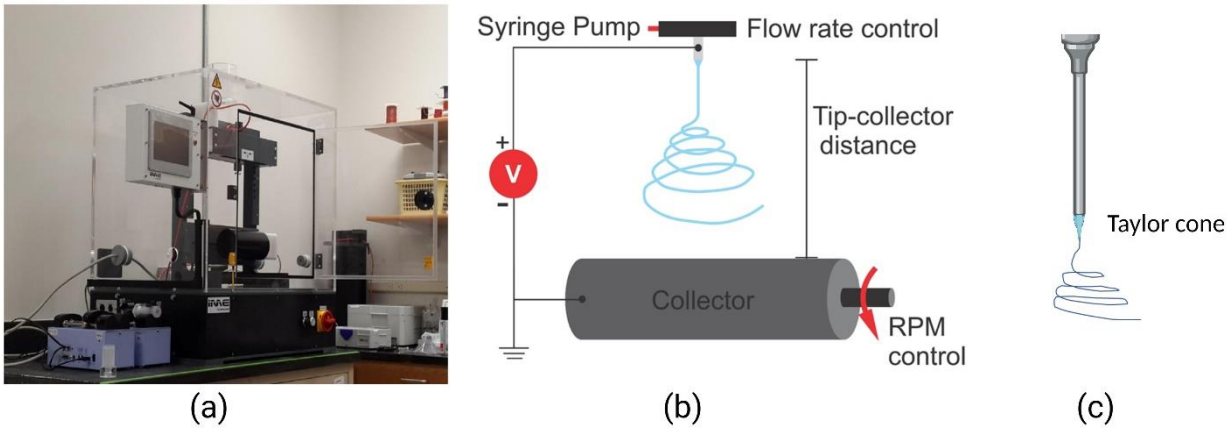

Figure 2. Electrospinning setup. (**a**) An electrospinning benchtop model (IME Tech EC-Dig); (**b**) an illustration of the electrospinning process showing the nozzle tip and rotating collector; (**c**) an illustration of the Taylor cone at the tip of the nozzle. Adapted with permission from [102].

2. Nanofiber Structure and Properties Affecting Outcomes in Engineered Tissues

2.1. The Morphology of Nanofibers Influences Tissue Growth

2.1.1. The Alignment and Pore Size of Nanofiber Scaffolds Positively Influence Myogenic Differentiation

The in vivo myogenic environment is comprised of both nanoscale collagen fibrils and aligned microscale basal lamina tracks. Spatial cues, such as nanofiber alignment and porosity, are significant in determining the fate of stem cells toward muscle. The positive influence of alignment on muscle differentiation has been widely explored [3,70–77]. Muscle fibers are aligned along an axis and are formed by a single cell [33]. Aligned scaffolds mimic the microenvironment of native muscle tissue, as well as increase bulk modulus and improve surface wetting [34]. Nanofibers can be aligned to create myogenic differentiation outcomes similar to that of micropatterned substrates. Myofibers grown on aligned polycaprolactone (PCL) nanofibers, for example, show alignment analogous to that of micropatterned PDMS, with muscle fibers aligning within 20° of nanofibers, exactly as in micropatterned PDMS [3]. Such scaffolds create muscle fibers with a myosin-heavy chain (MyHC) molecule content 10-fold greater than randomly oriented fibers. Aligned nanofibers increase the fusion index and myotube length of randomly oriented poly(hydroxybutyrate) PHB in H9c2 rat myoblasts, and C2C12 myoblasts form 600 µm myotubes in aligned PHB [103]. MyHC increased 8-fold in C2C12 cells differentiated on aligned 2:1 PCL, i.e., chitosan nanofibers compared to 2D films of the same composition [35]. Fujie et al. (2015) showed that myoblasts can be spatially coordinated and differentiated on aligned nanoribbons [104]. Alignment can also create scaffolds with moduli, more appropriate for myogenesis than their randomly oriented counterparts [35]. Studies recapitulating the nano and microscale features of native muscle with electrospinning and lyophilizing have directed myogenic differentiation and created dense myotube bundles [105].

A high porosity positively affects myogenic cell infiltration, and subsequent differentiation. Recent studies have shown the need for at least 80% porosity, as well as alignment, for directing muscle growth, especially in thick scaffolds [106]. Porosity as high as 97% has facilitated aligned myogenesis [107]. Large-pore-size scaffolds have treated volumetric muscle loss (VML) defects in vivo [30,31]. Kawano et al. (2013) showed that pore sizes similar to cell size leads to the myospecific differentiation of hMSCs, and even further, myodifferentiation can be achieved with a fiber size smaller than the cell size [29]. If pores increase in size beyond 20 µm and the fiber diameter increases as well, cells may grow

along fibers instead of in a 3D configuration, which could hinder growth and differentiation [30]. The structure of pores can also positively influence myogenesis, with parallel pores of 20 µm to 50 µm width, allowing for the parallel arrangement of myotubes within pore structures. These parallel pore scaffolds achieved in vivo compatibility with force generation in regenerated muscle [31]. Porosity can aid in promoting self-alignment of the muscle tissue, as well as aid in nutrient and waste transport in cell culture. Such pores can be achieved in electrospun mats through salt-leaching, laser-ablation or sacrificial polymer addition. Porosity can also be altered through processing changes via the influence of the fiber diameter. Evidence of correlation between fiber diameter and muscle differentiation is conflicting, which could be due to the unpredictable ways in which pore size is influenced by the fiber diameter [30,32,108,109]. Narayanan et al. (2020) [30] showed that on aligned matrices, larger fiber diameter led to greater alignment, elongation, spreading, and differentiation of myoblasts (Figure 3). Further research controlling for fiber diameter to relate myogenesis and pore size is needed. The development of engineered muscle tissues and in vitro muscle analogs for the repair and modeling of muscular wounds, muscular dystrophy, and degenerative diseases could serve as suitable models for drug testing and in vitro studies.

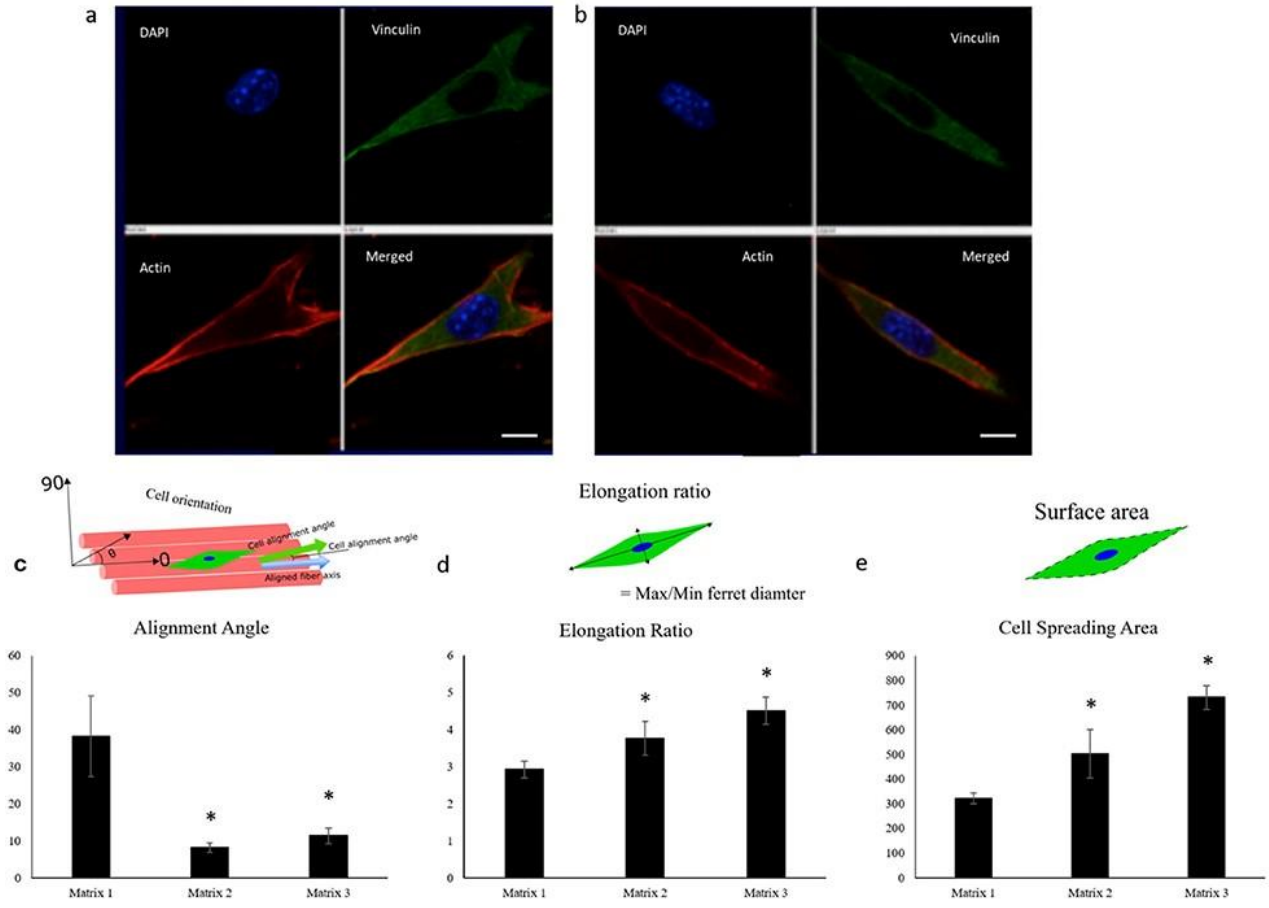

Figure 3. Confocal images of C2C12 cells showing elongation 2 h post-seeding on matrices of (**a**) 335 nm and (**b**) 3013 nm average fiber diameter, demonstrating the ability of myoblasts to respond to fiber diameters (red, actin cytoskeleton; blue, nuclei; green, vinculin). Scale bar: 10 µm. Quantification of (**c**) alignment angle, (**d**) elongation ratio, and (**e**) cell spreading area of seeded myoblasts 2 h post-seeding, showing enhanced myoblast alignment, elongation ratio, and cell spreading area on matrices spun from 20% (Matrix 1), 30% (Matrix 2), and 40% (Matrix 3) PLGA w/v solutions. $n \geq 4$ images for each sample. * $p < 0.05$ compared to Matrix 1. Image reproduced with permission from Narayanan et al. (2020) [30].

2.1.2. Fiber Morphology Directs Osteogenesis

It has been widely shown that bone cell maturation can be controlled by changes to nanofiber morphology [88–96,110–112]. Simon et al. (2011) and Kumar et al. (2011) showed that nanofiber matrices are unique in their ability to direct osteogenesis of stem cells by providing fibrous adhesion sites and forcing elongated and highly branched morphologies similar to that of mature osteocytes [113,114]. Such studies showed that nanofibers alone induced morphological changes in a manner similar to osteoinduction cell culture media. Kumar et al.'s study (2011) particularly showed that of the many scaffold types, including salt-leached, gas-foamed, phase-separated, 3D-printed and electrospun, only electrospun nanofiber scaffolds were able to differentiate the human bone marrow stromal cells (hBMSCs) down an osteogenic lineage without osteogenic supplements, irrespective of polymer chemistry. Fibers may drive osteogenic differentiation through the control of cell morphology, whereby the 3D microenvironment of the fibers enables cells to attain a more 3D morphology [115]. Fiber morphology also affects the shape and function of intracellular organelles, including the nucleus, mitochondria, and peroxisomes [116]. There is evidence that changes in substrate topography that change the cell shape and nuclear shape lead to changes in chromosome positioning, gene expression and protein synthesis [117,118]. Further, cell morphology may serve as an early indicator of an osteogenic response to fiber scaffolds [119,120].

It has been shown that aligned nanofibers cause higher osteoinduction than random microfibers (Figure 4) [121]. It has also been shown that a larger micron-scale fiber diameters of both poly L-lactic acid (PLLA) and Poly D,L-lactic acid (PDLLA) lead to a higher proliferation, aspect ratio and alkaline phosphatase (ALP) production of a clonal murine cell line of immature osteoblasts derived from mice (MC3T3-E1) compared to those cultured on nanofibers [36]. Aligned fibers have been shown to significantly upregulate calcium deposition of bone marrow stromal cells and alkaline phosphatase of preosteoblasts [122]. Efforts to recapitulate the native 10–300 nm aligned collagen fibers, upon which osteoblasts adhere and mineralize, were made by electrospinning aligned bio-based materials and showed high osteoconductivity [123]. Chen et al. (2013) created 3D multilayered constructs in which five layers of aligned and randomly oriented nanofibers, pre-seeded with pre-osteoblasts, were overlaid to mimic the structure of in vivo tissues [23]. These structures were successful in inducing osteogenesis compared to randomly oriented scaffolds. Aligned nanofibers can also increase stiffness and toughness, which can be beneficial to osteogenesis and will be explored in further sections [37]. However, the underlying mechanisms responsible for aligned fiber-related osteoinduction remains unclear. Some studies have shown no influence of aligned nanotopography on osteogenic stem cell fate [124–126], while others have shown that aligned nanotopography upregulates osteogenic stem cell fate [23,123,127].

Ultimately, mimicking hierarchical native conditions with morphological changes to nanofibers positively influences osteogenesis. Whether this must be through aligned fibers, random fibers, or a combination of both, requires further investigation. There have also been conflicting studies on nanofiber diameter impact on osteogenesis. Difficulties arise in linking nanofiber morphology properties to osteogenesis due to the many other variables influencing osteogenesis. For example, intercellular force, cell shape, and cell density heavily influence osteogenesis [108,128]. Other material properties, such as mechanical properties and surface characteristics, also play a significant role in influencing osteogenesis, which will be explored in the later sections.

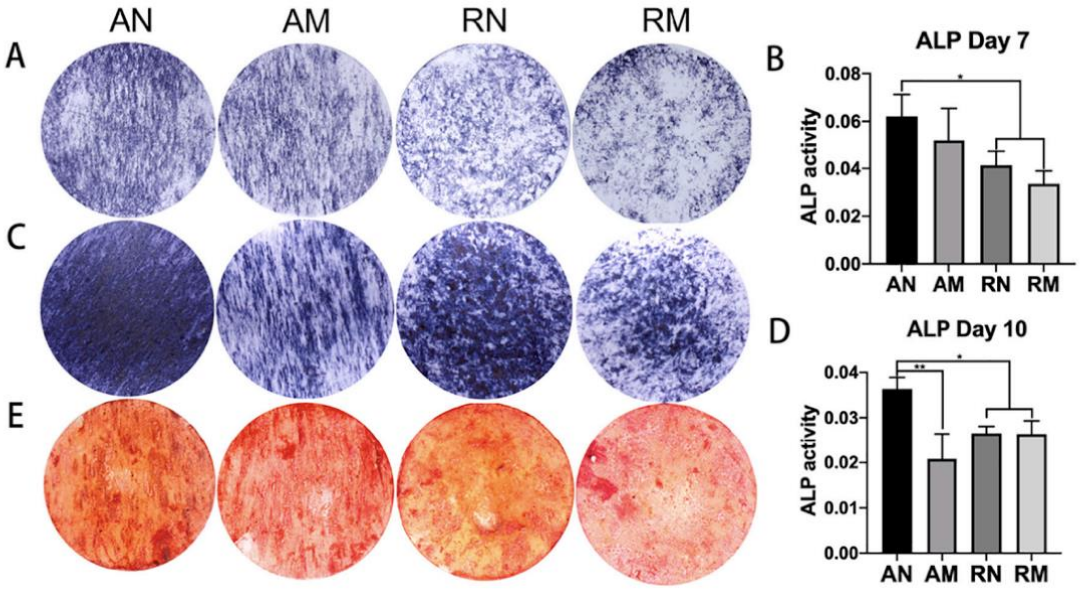

Figure 4. ALP staining and semi-quantitative analyses at day 7 (**A**,**B**) and day 10 (**C**,**D**), showing a higher ALP activity using aligned nanofibers, compared to randomly oriented fibers and microfibers (** $p < 0.01$, * $p < 0.05$); and ARS staining and semi-quantitative analysis at day 21 (**E**). Image reproduced with permission from Xie et al. (2021) [121].

2.2. Surface Characteristics of Nanofibers Influence Tissue Growth

2.2.1. Smooth Nanotopography and Biological Cues Influence Myogenesis

For the differentiation of muscle cells, it has been shown that smooth features at the nanoscale level positively influence myogenesis [98,99]. It has also been shown that biological cues, both through surface modification and the addition of biopolymers, positively influence myogenesis. In 2D films with random nano- and microtopography, low surface roughness positively influences myogenesis [129]. Hu et al. (2011) showed sensitivity of C2C12 mouse muscle cells to nanometer-scale surface roughness differences caused by the addition of tropoelastin to silk. Shin et al. (2015) showed that micron-level decreases in surface roughness through the addition of graphene oxide and collagen to randomly oriented PLGA fibers caused increases in attachment, proliferation, and myogenic expression of C2C12 cells [130]. While randomly oriented nanorough features on 2D substrates show a negative correlation with myogenesis, in aligned micropatterns, there is a positive correlation between roughness and myogenesis [131]. Nanoroughness may interrupt the controlled alignment of muscle fibers in 2D and randomly oriented microenvironments. However, nanoroughness also decreases contact angles with cells, which can positively influence differentiation. The contact angle effect of nanoroughness may dominate in aligned microenvironments, thus assisting in myogenic differentiation on aligned scaffolds. This would explain the synergistic effect of alignment and nanoroughness in a study conducted by Patel et al. (Figure 5) (2020) [132]. Yeo et al. (2019) used aligned nanofibers to directly enhance surface topology of 3D-printed PCL struts, and further used poly vinyl alcohol (PVA) leaching to create fibrillation mimicking the hierarchical topography of native muscle, significantly enhancing myogenesis compared to less realistic controls [133]. The influence of nanorough nanofiber surfaces on myogenesis has not been studied, but may show a synergistically positive effect on muscle growth. Though graphene oxide has been shown to enhance surface roughness for myogenesis on hydrogels, its use as a surface roughness modifier was overlooked in Jo et al.'s study (2020) of incorporating nanoscale graphene oxide or nGOs into polyurethane nanofibers [39,134].

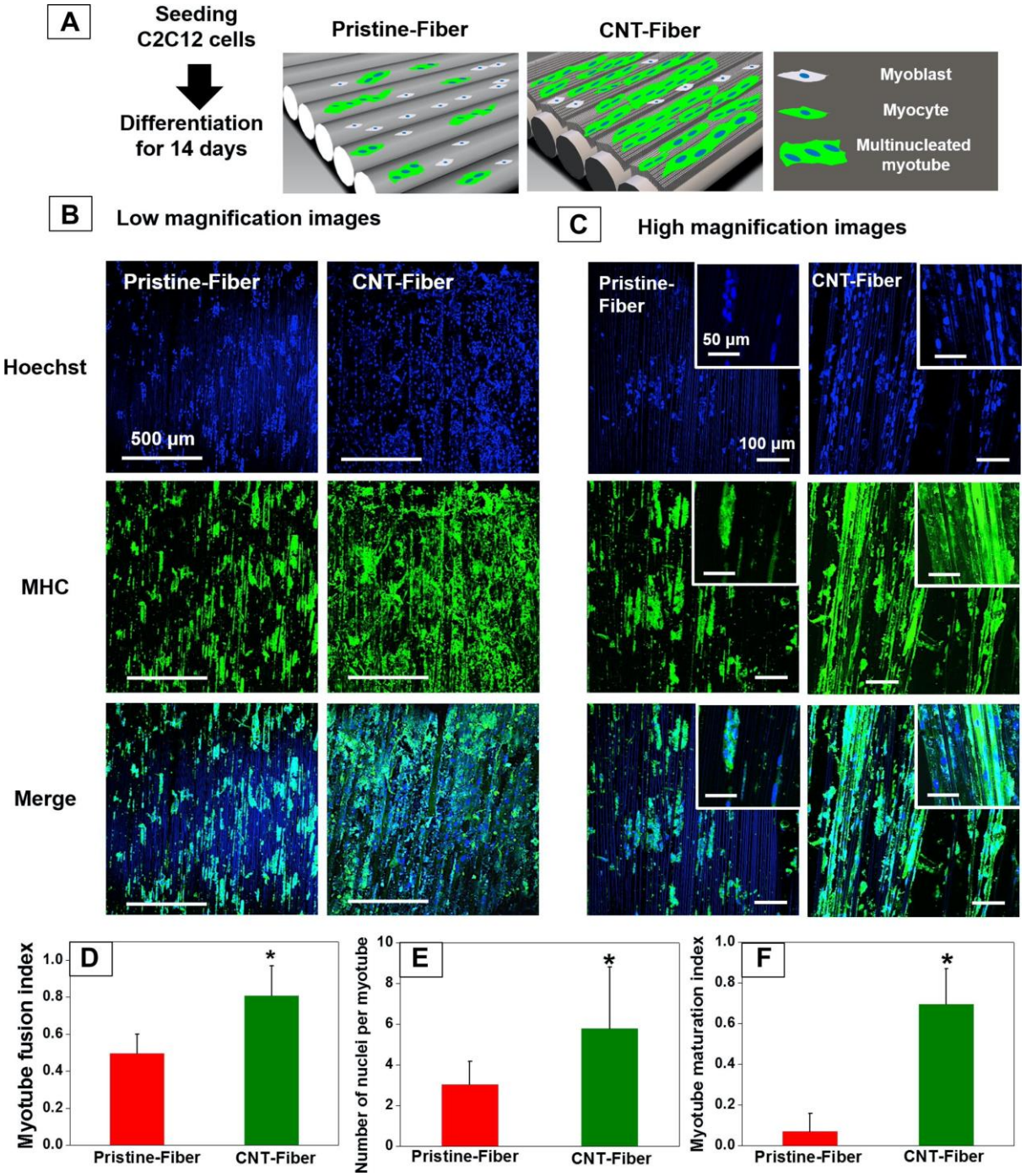

Figure 5. Effect of fiber alignment on myoblasts differentiating into myotubes. Schematic showing the formation of multinucleated myotubes over a 14-day period on pristine vs. CNT fibers (**A**). Magnification 10× (**B**) and 20× (**C**) images showing the formation of continuous multinucleated myotubes similar to muscle fiber bundles in cells grown on CNT fibers. Myotube fusion index (cells containing two or more nuclei/total cells in image) (**D**), number of nuclei per myotube, (**E**) and myotube maturation index (number of myotubes containing five or more nuclei/total number of myotubes) (**F**) showing a significantly higher fusion and maturation in myoblasts seeded on CNT fibers (* indicates $p < 0.05$). Image reproduced with permission from Patel et al. (2016) [132].

Biological cues also enhance the surface characteristics of scaffolds, promoting myogenesis. Biopolymers are often added to PCL to enhance the adhesion and differentiation of precursors. PCL is the most used polymer for tissue engineering due to its ease of

electrospinning, chemical stability, and bioresorbable properties [135,136]. Other polyesters, such as PLLA, poly lactic-co-glycolic acid (PLGA) and poly D-lactic acid (PDLA), have been employed for enhanced hydrophilicity and biocompatibility [137]. An addition of chitosan to PCL increases MyHC in differentiated human embryonic stem cells (hESCs) relative to pure PCL [138]. Myogenic factor 6 (MyF6) expression also doubled when chitosan was added. This is important as MyF6 is implicated in regulating skeletal muscle myogenesis and muscle regeneration. The benefits of biopolymer addition are mirrored in lyophilized chitosan/PCL samples, where increases in chitosan concentration also increase the myotube diameter [139]. This may be due to the increase in surface roughness imparted by chitosan addition, though chitosan addition at 12% and beyond may have compromised tensile strength to an extent unsuitable for muscle cell growth. Nanofibrous biopolymers can also be used to create biomimetic structures for the myogenic induction of C2C12s, as in Yeo et al.'s study (2019) [133]. In this study, nanofibrous alginate was electrospun onto micropatterned PCL struts to mimic the hierarchical structure of the basal lamina. Myotube length increased from 58.8 µm to 83.0 µm, the fusion index increased 3 fold, and the MyHC expression increased 14.6 fold on nanofiber-coated struts compared to nanofiber-free struts. Combinations of PCL with decellularized bovine skeletal muscle ECM electrospun into aligned fibers were shown to triple the proliferation of primary rat satellites when compared to pure PCL, as well as double the expression of the myoblast determination protein, MyoD [27], known to play a major role in muscle differentiation. PCL:ECM blended scaffolds were then shown to support MyHC regeneration in mice with VML [28]. Pure skeletal muscle ECM was highly successful in producing fully formed myotubes with dimensions of 25 µm width and 200 µm length [140]. Collagen, too, is a widely used biomaterial in electrospinning scaffolds for myogenesis. Collagen is integrated into electrospun myogenesis systems for a variety of reasons, including mechanical property optimization for compliance matching of smooth muscle [141], enhanced cytocompatibility [142], and adhesion [143] and enhanced myotube formation [144]. Biopolymers, such as chitosan and collagen, have potential as myogenesis-promoting additives to nanofiber scaffolds for their unique ability to enhance hydrophobicity, while decreasing nanoroughness [145]. Bioactive surface additions, such as platelet-rich plasma [146], arginine–glycine–aspartic acid (RGD) motifs [147], and recognition peptides [148] positively influence muscle differentiation by decreasing the cell contact angle, and activating integrin-mediated differentiation pathways. In conclusion, smooth adhesion sites on nanofibers play a role in upregulating myogenic differentiation. Rough sites on nanofibers, however, may be beneficial to myogenesis if such roughness is aligned. This is based on evidence of a positive influence of such roughness seen on other 3D and 2D substrates. In general, additives such as biopolymers which increase hydrophilicity will upregulate myogenesis, though further studies are needed to analyze how roughness may affect myogenesis purely through the modulation of hydrophilicity.

2.2.2. Surface Characteristics and Bone

Micro- and Nano-Rough Surfaces Positively Influence Osteogenesis

The importance of micro- and nanotopographical property influences on osteogenesis has been previously explored in several studies [145–150]. Generally, roughness can direct osteogenic differentiation, with higher nanoroughness upregulating osteopontin and ALP activity [149,150]. While nanoroughness upregulates osteopontin according to Jahanmard et al. (2020), microroughness has a positive effect on osteocalcin (Figure 6) [149]. Wang et al. (2012) showed that on crosshatched TiO_2 nanofiber scaffolds produced through sacrificial co-spinning with polyvinylpyrrolidone (PVP), microroughness, as well as a higher nanofiber diameter caused an increase in osteocalcin [151]. ALP activity, on the other hand, was more prominent on non-patterned low-roughness lower diameter nanofiber substrates. In this study, the roughness and nanofiber diameter were altered without affecting chemistry, suggesting that morphological properties of scaffolds, such as microroughness and nanofiber diameter alone, may influence osteogenesis. The downregulation

of early osteogenic marker ALP versus the upregulation of late markers, such as osteopontin (OPN) and osteocalcin (OCN) on micro and nano-rough surfaces, suggests that roughness drives the maturation of osteoblasts. In another study, nanoroughness was shown to selectively upregulate the expression of osteo differentiation markers [152]. For example, OCN, bone sialoprotein (BSP), and collagen A (Col1A) were upregulated by smoother nanofibers (Ra~14.3 nm), while OPN, BMP2, RUNX2, and ALP were upregulated by rougher (Ra~71 nm) nanofibers [152].Tissue engineering scaffolds for optimal bone maturation may benefit from using combined micro and nano-rough surfaces in nanofibers, or hierarchical nanoroughness. Such combined surfaces mimic bone structural hierarchy and have previously been explored for osteogenesis on non-nanofiber scaffolds, with certain substrates able to exhibit osteoconductivity without osteogenic supplements [153,154].

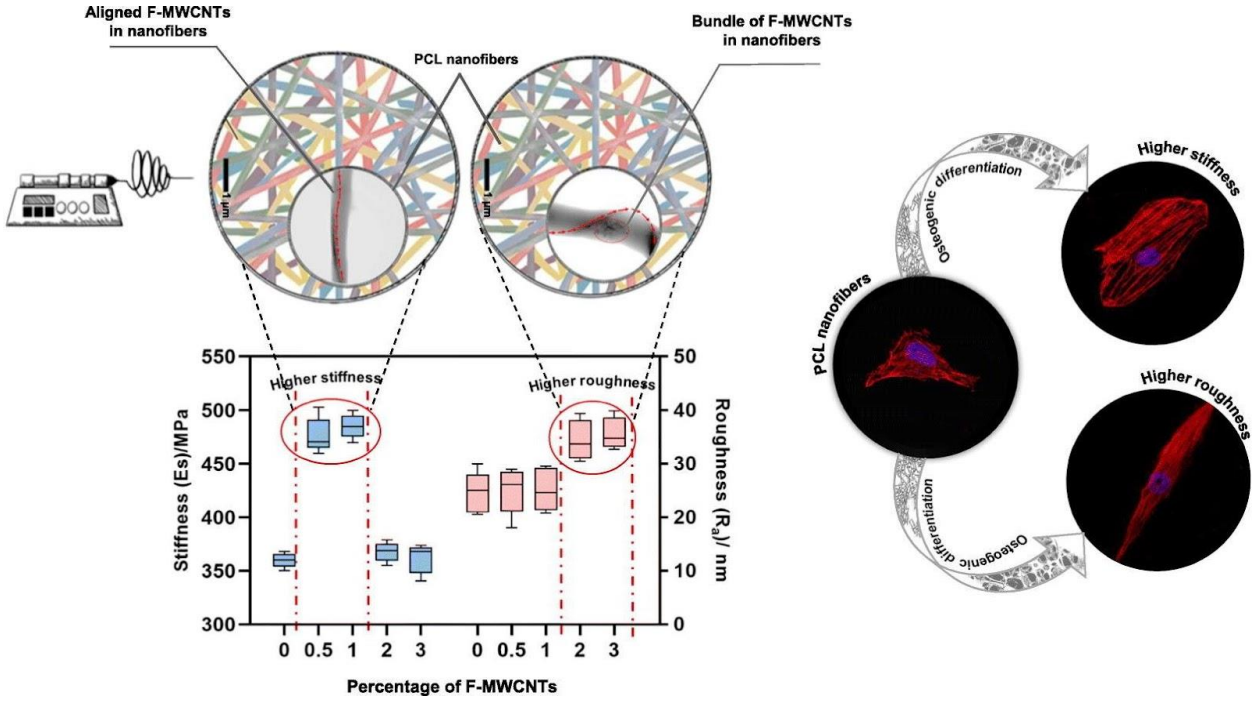

Figure 6. Addition of functionalized multiwalled carbon nanotubes (F-WMNCTs) allows for the tunability of both stiffness and roughness of nanofibers, which separately control spreading and elongation, ultimately leading to the expression of various osteo-specific differentiation markers. Image reproduced with permission from Jahanmard et al. (2020) [149].

Hydrophilic Surface Chemistry Improves Osteoconductivity of Nanofibers

Hydrophilic substrates allow cells to spread, adhere, and flatten, inducing osteogenesis [155]. Generally, surface chemistry which improves surface wetting properties will enhance osteogenesis. However, more research is needed to evaluate the influence of surface-bound functional groups on osteogenesis. For example, Sarkar et al. (2016) showed that in the NaOH-based hydrolysis of PCL nanofiber scaffolds, the carboxyl and hydroxyl groups were exposed on the nanofiber surface, causing a significant increase in water contact angle and decrease in osteogenic expression in hBMSCs. Ultimately, it was the cellular curvature, tortuosity, solidity, and aspect ratio that most significantly correlated with osteogenic differentiation. The area, perimeter, and circularity of cells were not significantly correlated with osteogenic differentiation, though in 2D culture environments, the spread and roundness were significantly correlated with osteogenic commitment. This suggests that the 3D architectures of nanofiber scaffolds are likely the dominating factor in determining the cell shape and differentiation, as opposed to surface chemistry [156]. Though exposing carboxyl groups may interfere with osteogenesis in vitro, studies have shown that negatively charged functional groups interact with calcium and phosphate

ions present in bodily fluids and facilitate hydroxyapatite crystallization, which may aid in osteogenesis [157]. Interestingly, studies involving plasma treatment cite resultant exposure of carboxyl and hydroxyl groups as adhesion promoters, and thus osteogenesis promoters [158]. It is more probable that the hydrophilic effect from creating oxygen functional groups is what drives osteogenesis. Cold atmospheric plasma treatment of PLGA drives osteogenesis through increased hydrophilicity of nanofibers, as well as the formation of micro/nano roughness. Plasma treatment also leads to improved viability through improved adhesion. Atyabi et al. (2016) showed a 2× improvement in cell viability via cold atmospheric plasma treatment of the scaffolds [159]. Plasma treatment may also improve adhesion of additional surface modifiers. Kooshki et al. (2019) used a plasma treatment followed by a lipopolysaccharide coating to enhance osteoconductivity of mesenchymal stem cells (MSCs) on PLLA [160]. Lipopolysaccharide promotes osteogenic differentiation by fortifying the activity of TAZ (transcriptional coactivator with a PDZ-binding motif), a transcriptional co-regulator which plays a key role in osteoblast differentiation, as mediated by the Wnt/β-catenin pathway [161]. The conjugation of amino acids aspartic acid (ASP) and glutamic acid (GLU) enhances hydrophilicity more than cold atmospheric oxygen [162]. Conducting both plasma treatment and the conjugation of GLU/ASP to PLGA nanofibers synergistically improves osteoconductivity of the scaffolds. ASP induces cell proliferation and osteogenic differentiation more than GLU, due to the role of ASP in integrin binding recognition and higher binding affinity for calcium ions by ASP. Surface wettability was enhanced through the addition of chitosan and a polydopamine layer on PLLA nanofibers, leading to improved cell spreading and more accurate recapitulation of in vivo conditions, leading to enhanced osteogenesis [163]. Similar synergistic results were observed with the addition of gelatin and hydroxyapatite to PLGA [164]. At 60% concentrations, medicinal *Cissus quadrangularis* extract in PLLA increased hydrophilicity of MSCs and doubled ALP activity and calcium deposition [165]. Nano-hydroxyapatite (nHA)-coated nanofibers mimic the bone extracellular matrix, which is composed of collagen type I nanofibers mineralized with nanosized calcium phosphate crystals. In experiments with polydopamine and nHA-coated PCL nanofibers, the water contact angle was reduced to 0° and osteoinduction was enhanced [166]. Similar results were seen in nHA-coated PLLA nanofibers, which induced bone formation 10 weeks after subcutaneous implantation in mice, showing that nHA can induce bone formation in absence of exogenous agents or cells [167].

The addition of peptides and hydrophilicity enhancers significantly upregulate osteoinduction. The formation of nanorough or microrough features for cell adhesion is essential for promoting bone cell differentiation. Studies exploring how roughness can be dynamically tuned to fit the needs for biological cues throughout bone cell differentiation are needed to further optimize osteoinductive nanofibers.

2.3. Mechanical Properties and Crystallinity

2.3.1. Muscle Differentiation Is Supported by Elastic, Conductive, and Crystalline Scaffolds

Scaffold crystallinity and mechanical properties play an important role in regulating myogenesis. Crystallinity directly influences mechanical properties of scaffolds and may also have an independent role in enhancing the conductivity of scaffolds for improved myogenesis. Myogenic differentiation depends highly on the microenvironment elasticity being 8–17 kPa [168]. The subsequent proliferation, elongation, alignment and myofibrillogenesis of myoblasts [169] occurs in an even smaller range of microenvironmental stiffness of 11–15 kPa, with the striation of cells decreasing significantly outside this range [170]. It is important to note that this mechanical testing was conducted on individual nanofibers using AFM nanoindentation, while more conventional bulk tensile testing of nanofiber material often yields stiffness in the megapascal (MPa) range. In differentiating stem cells into muscle tissue on nanofibers, scaffolds which most successfully induce differentiation fall within the bulk modulus range of 10–15 MPa [27,38,134,138]. The elastic modulus of 17 kPa has been shown to dictate the differentiation of mesenchymal stem cells into muscle cells positive for alpha-actin [148], replicating the modulus effect seen in Engler

et al.'s study (2004). Patel et al. (2020) were able to mix high-modulus (75 MPa) PCL and low-modulus decellularized muscle ECM (1 MPa) to achieve scaffold mechanical properties ideal for myogenesis, with the added benefit of including ECM pro-myogenic biological cues [9]. High elasticity, high strain at break, fast stress relaxation rate, and tensile strength of 5–15 MPa generally favor myogenesis [38,39,171]. Exceptions to certain rules may occur as in, for example, Xu et al.'s study (2014) employing multiwalled carbon nanotubes [171]. In this study (Figure 7), an improved conductivity of scaffolds was able to enhance myogenesis, despite moduli in the range of 70–100 MPa. This highlights the importance of scaffold crystallinity properties in dictating myogenesis, as conductivity and crystallinity are intimately linked.

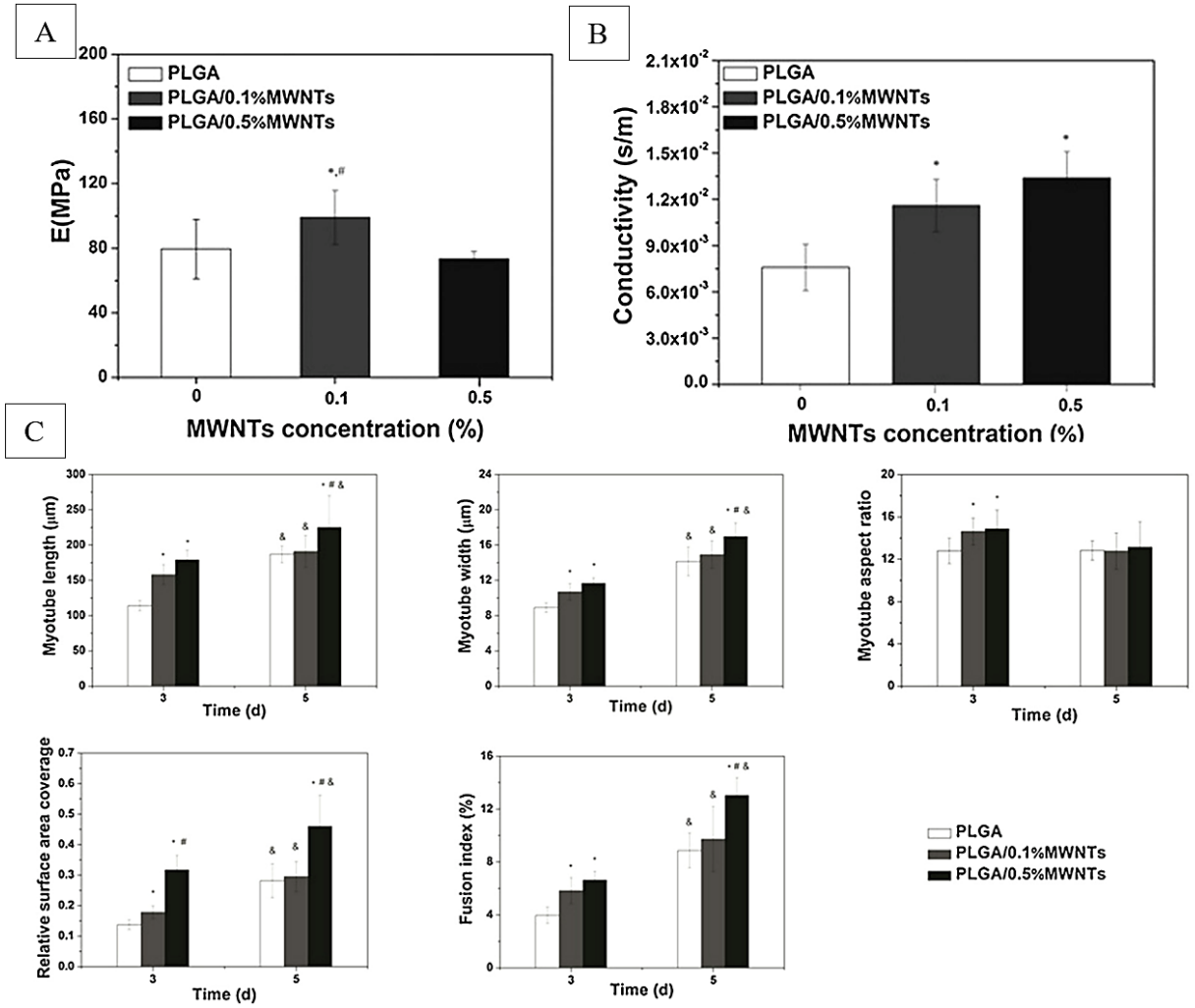

Figure 7. Young's moduli (**A**) and conductivity (**B**) properties of PLGA nanofibers, and (**C**) corresponding quantitative analysis of morphological indexes of myotubes on days 3 and 5, including myotube length, width, aspect ratio, surface coverage, and fusion index (n = 10; *, #, &: $p < 0.05$; *: compared to PLGA; &: compared to day 3; #: compared to PLGA/0.1%MWNTs). Adapted from [171].

Through nanofiber crystallinity changes, conductivity, elasticity, and strength can be altered to create materials appropriate for muscle stem cell differentiation. Surface wettability is also an important material parameter which positively influences myogenic differentiation. Bloise et al. (2018) altered wetting and mechanical properties of electrospun poly(butylene 1,4-cyclohexanedicarboxylate) through the addition of PEG-like co-units, decreasing crystallinity and increasing amorphous regions, leading to increased surface

wetting and elasticity, and decreased stiffness. These changes made the scaffolds suitable for successful regeneration in murine models [38]. Jana et al. (2014) showed that the addition of chitosan from 4% to 8% to PCL increased the scaffold crystallinity and resulted in an increased myotube diameter of cultured C2C12 cells [139]. In a separate study, the addition of chitosan from 0% to 4% decreased the crystallinity in scaffolds, but improved myogenesis [105]. Myogenesis is controlled by many factors, and the biopolymer concentration can alter crystallinity to optimize the scaffold systems for myogenesis. Increased crystallinity of graphene oxide nanoparticles through APTES ((3-Aminopropyl)triethoxysilane) treatment had a positive effect on myogenesis, improving conductivity, wetting, and elasticity, as well as the stress relaxation capacity of polyurethane nanofibers [39]. In this study, a significant improvement in myogenic differentiation was observed on fibers containing 8% nanographene oxide, the only observably conductive sample in the experiment. Crystallinity, it is apparent, can play an important role in supporting myodifferentiation if the impact on mechanical elasticity and recovery is not too great. In general, preliminary properties of solution stability must first be met by nanofibers to support myogenesis. Uribe-Gomez et al. (2021) showed, for example, that of the fourteen PCL-PU (polyurethane) block copolymers synthesized, only one medium-crystallinity polymer was able to maintain stability in phosphate-buffered saline or PBS, and support myogenesis [172]. Once such stability is achieved, a polymer with both elasticity and conductivity is the most ideal for optimized myodifferentiation.

Scaffolds can be optimized for myodifferentiation through an enhancement of elasticity, crystallinity, and conductivity. The interplay and hierarchy of these variables, with regards to influencing myogenesis, is yet to be confirmed empirically. A summary of recent innovations relating nanofiber scaffold materials and respective mechanical, electrical, and crystallinity properties studied for muscle differentiation, is listed in Table 1.

Table 1. List of the recent innovations relating fiber-based scaffolds for engineering muscle tissue based on biophysical properties of the scaffold.

Material Used	Type of Electrospinning	Mechanical Properties	Electrical/Crystallinity Properties	Result of Tissue Growth	Reference
PCL nanofibers and PEG hydrogel	Direct electrospinning (rotating drum)	Aligned and randomly oriented scaffolds studied		Increased myotube growth, alignment, and nuclear aspect ratio from aligned fibers	[3]
PHB	Direct electrospinning (rotating drum)	Higher stiffness and strength in aligned nanofibers		Aligned nanofibers decrease proliferation, but increase differentiation markers of muscle cells	[78]
2:1 PC–chitosan	Direct electrospinning (rotating drum and parallel electrodes)	Higher stiffness and strength in aligned nanofibers		Increased myodifferentiation in aligned nanofibers	[79]
PLGA	Micropatterning and spincoating	Multilayer, parallel and orthogonal nanoribbons fabricated		Aligned nanoribbon biolayers upregulated myogenic markers and led to muscle maturation moreso than random or single-layer nanoribbons	[80]
5:2 PCL–chitosan	Direct eletrospinning (parallel electrodes)	Nanofiber/microchannel layered structures fabricated		Aligned nanofibers perpendicular to aligned microchannels caused the highest degree of myodifferentiation	[71]

Table 1. *Cont.*

Material Used	Type of Electrospinning	Mechanical Properties	Electrical/Crystallinity Properties	Result of Tissue Growth	Reference
1:1 Bovine muscle ECM–PCL	Direct electrospinning (rotating drum)	Higher stiffness and strength in aligned, non-ECM nanofibers		Addition of ECM enhanced myodifferentiation, despite the loss of mechanical properties	[73]
PLGA	Direct eletrospinning (parallel electrodes)	Mechanical properties similar for scaffolds 300–3000 nm		Larger fiber diameter upregulates muscle-specific markers	[83]
Carbon nanotubes	Dry drawing from aligned CNT forest		Aligned CNTs showed higher conductivity than randomly oriented and flat substrates	PAX7 and MyF5 were upregulated in aligned CNT substrates	[92]
PLGA/graphene oxide/collagen	Direct electrospinning (rotating drum)	Increased strength, decreased stiffness and elongation with collagen and GO	Enhanced crystallinity with GO addition	Enhanced attachment, proliferation, and MyHC expression in fibers with GO and collagen	[99]
Alginate/PCL	Direct electrospinning (parallel rotating drums)	~2 MPa alginate nanofiber-coated PCL strut with a high roughness fabricated		Myotube length and MyHC expression improved dramatically in hierarchal strut structures	[102]
Polyurethane/graphene oxide	Direct electrospinning (rotating drum)	Increased strength and stiffness from graphene oxide addition	Conductivity enhanced with APTES and GO addition at 8%	Collagen and GO addition increased adhesion, proliferation, and myogenic differentiation	[103]
PBCE–PEG copolymer	Direct electrospinning (rotating drum)	Decreased stiffness and strength, increased elasticity, with more PEG units		Increased PEG units led to more muscle-like elastic properties and increased myodifferentiation	[135]
PLGA/multiwalled carbon nanotubes	Direct electrospinning	Decrease in elasticity and strength, with increased MWCNT addition beyond 0%	1.3×10^{-2} s/m conductive fibers fabricated	Increased myotube length, diameter, and proliferation, with increased MWCNT concentration	[136]
Polyester polyurethane with glycol chain extenders	Touch-spinning	Recovery and elastic modulus increased, with increased urethane segment addition	Crystallinity customized with urethane segments and glycol chain extenders	PCL–urethane–butanediol chain extender ratio necessary to optimize for successful myocyte growth on nanofibers	[137]

Abbreviations: PCL, polycaprolactone; PLLA, poly L-lactic acid; PEG, polyethylene glycol; GO, graphene oxide; PHB, polyhydroxybutyrate; PC, phosphatidylcholine; PLGA, poly lactic-co-glycolic acid; ECM, extracellular matrix; CNT, carbon nanotubes; PAX7, paired box 7; MyF5, myogenic factor 5; PBCE, poly(butylene 1,4-cyclohexanedicarboxylate).

2.3.2. Bone Differentiation Prefers Crystallinity and Conductivity, Followed by Stiffness and Strength

It has been shown in nanofiber scaffolds that a high tensile modulus of 20 MPa to 60 MPa is beneficial for osteogenesis [149,173,174]. For example, Nam et al. (2011) created PCL nanofibers with and without a polyether sulfone (PES) core, thereby forming nanofibers of 7.1 MPa modulus and 30.6 MPa modulus for the PCL and PES-PCL core-shell nanofibers, respectively. Murine MSCs were seeded, and the softer pure-PCL fibers led to the upregulation of chondrocyte-specific Sox9, Co12a1, and Acan, and increased GAG

production, while stiffer PES-PCL core-shell nanofibers led to the upregulation of osteocyte-specific RUNX2, Alp, and Oc [173]. Jahanmard et al. (2020) showed that functionalized multiwalled carbon nanotubes (F-MWCNTs) increase nanofiber stiffness at loadings of 0.5% to 1% F-MWCNTs. A higher stiffness increased the expression of osteocalcin while a higher nanoroughness increased the expression of osteopontin, indicating that unique signaling pathways can be independently controlled by material stiffness and material topography [149]. Chitosan and polydopamine have been used to synergistically enhance tensile strength and Young's modulus to the Gigapascal (GPa) range, as well as surface wetting conditions, to enhance the osteogenesis of MC3T3 cells [163]. Hydroxyapatite and graphene oxide (GO) incorporated into PLGA showed synergistic increases in proliferation, calcium deposition, adhesion, and expression of ALP, osteopontin and RUNX2 in MC3T3-E1 murine preosteoblasts by increasing the tensile strength and modulus [174]. With the tensile strength of cancellous bone being 10.4 GPa and cortical bone being 18.6 GPa, a stiff microenvironment will promote osteogenesis over a less stiff one with other properties held constant [175].

Nanofiber scaffolds loaded with magnetic nanoparticles, bioactive ingredients, or additives to enhance material crystallinity can often increase osteogenesis, despite drastically hindering mechanical properties [40,144,165,176,177]. Crystallinity has been shown to be a significant driver of osteogenesis in many studies [117,139,147,148], but few have successfully decoupled their effect on mechanical properties. The addition of graphene oxide (GO) to nanofibers, for example, was shown to decrease tensile strength more than 10 fold, as well as decrease stiffness, but positively influence osteogenesis (Figure 8 [40]. Using almost equal parts of GO and polymer, Saburi et al. (2019) saw more of an improvement in the proliferation and ALP expression of hiPSC cells than studies using both GO and hydroxyapatite, despite negatively impacting mechanical properties [40,174].

Graphene oxide has been shown to increase the crystallinity of polyvinylidene fluoride (PVDF) nanofibers, and introduce crystalline regions, which would explain this impact on osteogenesis [178]. The addition of nanoclay to PCL nanofibers similarly decreased the strength and stiffness, but increased crystallinity, as evidenced by X-ray diffractometer (XRD) and differential scanning calorimetry (DSC) measurements [150]. Nanoclay and graphene oxide do not always decrease the strength and stiffness of electrospun scaffolds; studies have shown the opposite effect when other base polymers are employed [179,180]. Yao et al. (2020) showed that the addition of graphene oxide to PVDF drastically up-regulated osteodifferentiation compared to pristine PVDF. These matrices produced such outcomes despite having a relatively low strength and stiffness, likely due to their increased crystallinity. Studies such as these demonstrate the need for further investigation into the mechanisms involved in crystallinity-modulated osteoinduction. Studies have shown the positive impact of crystallinity on osteogenesis in 2D films, but have not been repeated for 3D and nanofiber systems [181]. Little is known about the influence of crystallinity on osteogenesis, and some studies have shown amorphous morphology, not crystalline morphology, to be responsible for bone cell growth [182,183]. The maturation of reinforcing bone starts with an amorphous precursor, amorphous Ca-phosphate (ACP), which converts to crystalline hydroxyapatite. Recent studies by Muller et al. (2020) showed that, due to this, the amorphous polyphosphate stimulated osteogenesis more than crystalline polyphosphate [183]. These contradictions are likely due to present limitations on scaffold technology. Scaffolds capture only a snapshot of cell maturation microenvironments. More research is needed on scaffolds with dynamic properties to correspond to the morphological changes of tissue over time.

Osteo-differentiation is highly sensitive to mechanical properties, with stiffness and strength positively correlated with osteogenic markers. However, this research has shown that osteoconductive additives such as hydroxyapatite, graphene oxide, polydopamine, and carbon nanotubes will promote bone growth despite negatively impacting mechanical properties. This is likely due to increases in hydrophilicity, conductivity, or combinations of both. Thus, newly fabricated electrospinning materials should pursue integration with such

additives or maximization of wetting and electrical conductivity properties. Fiber-based constructs may be useful for musculoskeletal applications. A device for rotator cuff repair that is made from electrospun fibers is undergoing testing in humans [184]. A summary of recent innovations for nanofiber scaffold materials and respective mechanical, electrical and crystallinity properties studied for bone differentiation, is listed in Table 2.

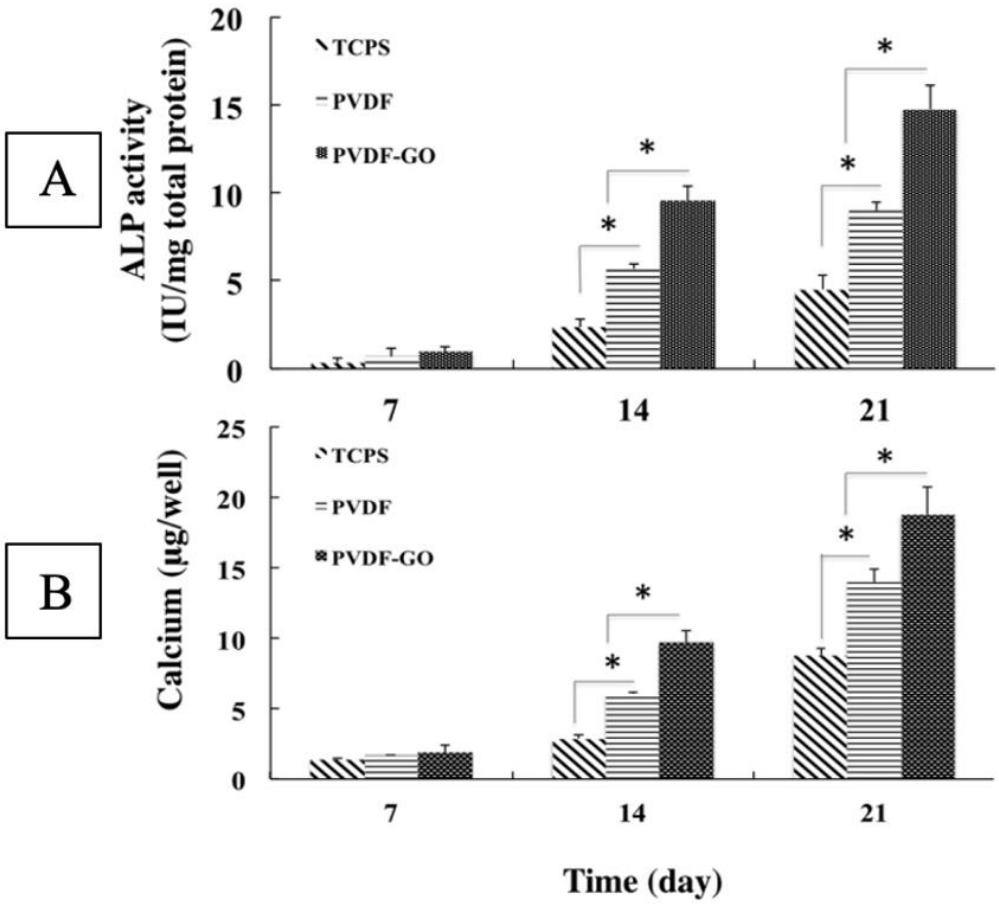

C

Group	Peak stress	Peak strain	Tensile strength	Tensile strain	Tensile modulus
PVDF	1.65 MPa	10.86%	1.18 Mpa	2.4%	49.16 Mpa
PVDF-GO	1.14 Mpa	52.1%	0.1 Mpa	1.6%	6.25 Mpa

Figure 8. Osteogenic differentiation of iPSCs, as shown via ALP (**A**) and calcium (**B**) expression, with evidence of significant (* indicates $p < 0.05$) upregulation due to the addition of graphene oxide, despite a reduction in strength and stiffness (**C**). Adapted from [40].

Table 2. List of the recent innovations relating fiber-based scaffolds for engineering bone tissue based on biophysical properties of the scaffold.

Material Used	Type of Electrospinning	Mechanical Properties	Electrical/Crystallinity Properties	Result of Tissue Growth	Reference
Carbon nanotubes	Dry drawing from aligned CNT forest		Aligned CNTs showed higher conductivity than randomly oriented and flat substrates	Flat surfaces upregulated osteogenic markers (RUNX2, osteopontin)	[92]
PCL and functionalized multiwalled carbon nanotubes (F-MWCNTs)	Direct electrospinning	Increased stiffness at 0.5–1% F-MWCNT loading, decreased at 2–3% loading	CNTs known to increase conductivity	Osteogenesis induced by F-MWCNTs, with osteocalcin upregulated by increased stiffness	[116]
PCL and nanoclay	Direct electrospinning	Decreased stiffness and strength with 1–a 10% addition of nanoclay	Crystallinity increased with the addition of nanoclay	Increased mineralization and ALP activity with 1% addition nanoclay	[117]
PCL shell with PES core	Coaxial Direct Electrospinning	Increased stiffness with the addition of a PES core		Increased osteoinduction with a stiffening PES core	[138]
PLLA/chitosan/polydopamine	Direct electrospinning	Increased stiffness and strength through the addition of chitosan and polydopamine		Increased osteoinduction through a synergistic addition of chitosan and polydopamine	[129]
PLGA/graphene oxide/hydroxyapatite	Direct electrospinning	Decreased stiffness and strength with HA addition, increased stiffness and strength with GO addition	Conductivity increased due to HA and GO	Increased osteoinduction with addition of HA and GO	[139]
PVDF/graphene oxide	Direct electrospinning	Decrease in peak stress, strength, and stiffness with graphene oxide addition	Piezoelectric properties exhibited by PVDF	Increased osteoinduction with addition of GO	[144]

Abbreviations: PCL, polycaprolactone; RUNX2, runt-related transcription factor 2; PES, polyethersulfone; HA, hydroxyapatite; PLLA, poly L-lactic acid; PEG, polyethylene glycol; GO, graphene oxide; PLGA, poly lactic-co-glycolic acid; CNT, carbon nanotubes; PVDF, polyvinylidene fluoride.

3. Biological Requirements Affecting the Choice of Nanofiber Scaffolds

3.1. Skin and Wounds

Skin tissue is the largest organ of the human body, with a total surface area of more than 15,000 cm^2 and accounting for 5% of the total body weight. The skin, an ectodermal tissue, is the first line of defense and protects internal organs and tissues, such as muscle, bone from damage such as pathogens and chemical hazards, maintain isothermal conditions, and provides mechanical support for the optimal functioning of the body. The skin also acts as the primary sensory organs and an immunological mediator. Wound healing, skin tissue regeneration and restoration of the skin is a vast field with particular interest in scaffolds. Different materials have been demonstrated for use as scaffolds for skin tissues [82,185]. An example of PCL-PANi used as a scaffold for adult human dermal fibroblasts is shown in Figure 9 [82].

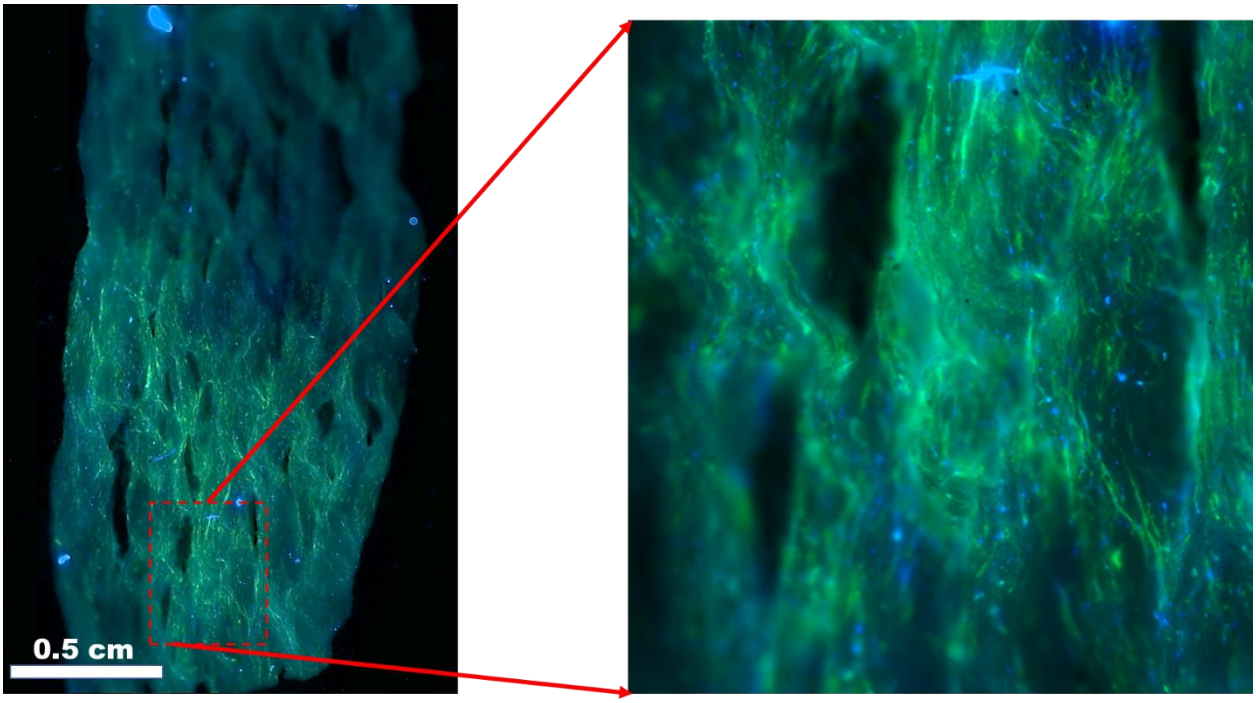

Figure 9. Adult human dermal fibroblast (HDFa) cells after 7 days of culture on polycaprolactone/polyaniline scaffolds. Blue: DAPI nuclei stain; green: Alexa Fluor® 488 Phalloidin F-actin filaments. Image courtesy of Samerender N. Hanumantharao, Michigan Technological University.

The skin is composed of three types of tissue layers, each having its own distinct morphological and mechanical properties. The epidermis is the outermost layer of skin that receives its nutrients from the dermis layer. The deepest layer of the Stratum Basale, also known as stratum germinativum, is one which divides and attaches to the basement membrane through hemidesmosomes. The epidermis renews itself constantly and is being replaced every 28 days due to the activity of keratinocytes present in this layer. This layer also contains melanocytes responsible for producing melanin. Above this layer lies a lining of spine-like cells of eight to ten cell layers called the stratum spinosum containing the dendritic cells. The stratum granulosum is three to five cell layers and contains keratohyalin granules, which are the keratin precursors and lamellar granules that help in cell–cell attachment. The stratum lucidum is a thin layer that contains the transformation of keratohyalin (eleidin). The stratum corneum is the outermost layer that is twenty to thirty cell layers thick made up of anucleate squamous cells from dead keratinocytes. This layer is present at differing thicknesses, especially in callused skin. This layer is embedded in a lipid matrix composed of cholesterol, and other free fatty acids, which helps water retention and acts as the first barrier. It also produces defensins through the Langerhans cells. The basal layer also contains the Merkel cells, oval shaped type I mechanoreceptors that are slow-adapting and found attached to the layer through desmosomes, Merkel disks which sense light touch, Pacinian corpuscles which sense deep pressure, Meissner's corpuscles which sense low-frequency stimulation, and Ruffini corpuscles which sense pressure. The dermis is connected to the epidermis through the basal membrane and has hair follicles, sweat glands, and somatic and autonomic nerves. The hair follicles also have smooth muscle fibers that are attached to the connective tissue sheath called the arrector pili muscles. This helps in controlling the sebaceous glands. The dermis is 1 mm to 2 mm thick and consists of a system of filamentous connective tissue with vasculature and nerve cells. The dermis provides elasticity to the skin tissue primarily due to the high elastin amount present in the tissue and mechanical support due to the loose collagen networks. The final layer is the hypodermis, which is composed of fibroblasts and adipocytes, providing mechanical and thermal insulation.

Fiber scaffolds could be useful as skin substitutes and wound dressings. An electrospun nanofiber dressing for wound care has been cleared by the Food and Drug Administration (FDA) for marketing in the USA, but clinical results have not yet been published [186,187]. A handheld electrospinning device has been developed for creating spray-on wound dressings that custom fit the patient's wound bed. This system is currently being tested on patients [188]. A summary of recent innovations relating nanofiber scaffold materials and respective mechanical, electrical and crystallinity properties studied for skin differentiation, is listed in Table 3.

Table 3. List of the recent innovations relating fiber-based scaffolds for engineering skin tissue based on biophysical properties of the scaffold.

S No.	Material Used	Type of Fabrication	Mechanical Properties	Electrical Properties	Cell Response	Reference
1	Nanocomposite PU/PCL scaffolds with GO	Direct electrospinning	• 3D porous structure • Increased fiber diameter	-	Increased hydrophilicity and biocompatibility	[189]
2	PCL, PGS and regenerated silk fibroin	Nozzle-free electrospinning	Tunable hydrophilicity/hydrophobicity based on PGS	-	Increased fibroblast attachment	[190]
3	Polyurethane/starch (hyaluronic acid)	Coaxial electrospinning	• Increased hydrophilicity due to HA • Complete degradation of scaffolds by week 3 • Adequate tensile strength	-	• Increased cellular attachment and proliferation of mouse fibroblasts in vivo • Presence of sebaceous glands in mice on day 14	[191]
4	PVA/glucose–reduced graphene oxide (GRGO)	Direct electrospinning	Addition of GRGO increased hydrophobicity and the diameter of fibers	-	Increased hemocompatibility and biocompatibility	[192]
5	Santa Barbara amorphous (SBA)-15–incorporated PVA with curcumin	Direct electrospinning	• Highly hydrophilic • Large surface area due to the presence of mesopores • Mesh-like topography	-	• In vitro drug release of curcumin • Increased wound healing activity in vivo	[193]
6	Core-shell PLA/kefiran	Direct electrospinning followed by air plasma treatment	Increased reinforcement due to presence of Kefiran improving tensile strength and crystallinity.	-	Increased biocompatibility and collagen production	[194]
7	Maltodextrin mixed with argi-nine/lysine/polylysine	Environmentally controlled direct electrospinning	Nanofibrous morphology Elastic and high breaking point	Negative zeta potential in fluids	• Accelerated healing of wounds in mice, vascularization of tissue • Antioxidant activity aided in healing	[195]
8	Polypyrrole/chitosan/ collagen	Direct electrospinning	Uniform fibrous structure Increase in polypyrrole-reduced diameter of fibers Adequate mechanical strength	Increased conductivity due to polypyrrole in the semiconducting polymer range	Increased cell adhesion, growth, and proliferation	[196]
9	PCL/gelatin/MgO preseeded with endometrial stem cells	Direct electrospinning	Increase in mechanical properties due to gelatin and MgO Increased porosity Release of Mg ions	-	The release of Mg ions and the structure of scaffolds aided in full thickness skin wound closure in mice.	[197]
10	Chitosan–PVA and silk seeded with differentiated keratinocyte	Co-electrospinning	• Increase in hydrophilicity • Smooth fibrous morphology • Hybridization and co-electrospinning processes increased mechanical characteristics of the scaffold		Increased cell adhesion The MSC-derived keratinocytes stimulated wound healing in mice	[198]

Table 3. *Cont.*

S No.	Material Used	Type of Fabrication	Mechanical Properties	Electrical Properties	Cell Response	Reference
11	Electrospun chitosan/nanocrystalline cellulose–graft-poly(*N*-vinylcaprolactam)	Direct electrospinning	• Increase in fiber diameter due to nanocrystalline cellulose-graft-poly(*N*-vinylcaprolactam) • Increased thermal stability • Increase in hydrophilicity	-	Increase in cytocompatibility and cell proliferation	[199]
12	Collagen–graphene oxide (Col–GO) scaffolds loaded with basic fibroblast growth factor (bFGF)	Coaxial electrospinning	Core-shell structure aids in release of bFGF, increased mechanical strength and degradation conducive to wound healing	-	Increased healing and skin regeneration in rats	[200]
13	PCL/gelatin and modified acetylated cellulose nanofibers	Direct electrospinning	Increase in ultimate tensile strength and reduction in degradation rates due to the addition of cellulose nanofibers	-	Increased cell adhesion and proliferation	[201]
14	Poly(ε-caprolactone)	Direct electrospinning with micro-stereolithography (μSLA)	Control over topography aided in fabrication of ridge-like structures such as native tissue	-	Increased stratification and skin-like formation due to the topography of scaffold	[202]
15	Janus nanofibers, rana chensinensis skin peptides (RCSPs), and silver nanoparticles (Ag-NPs)	Uniaxial electrospinning	Loading with RCSP and Ag-NP improved the hydrophilicity and mechanical properties, while also providing anti-bacterial activity	-	Accelerated wound healing characterized by re-epithelization	[203]
16	Corn peptides (CPs) with Janus nanofibers	Coaxial electrospinning	Increased hydrophilicity, biocompatibility, mechanical strength, and free-radical scavenging capabilities	-	Improved wound healing ratio with enhanced fibroblast proliferation and formation of hair follicles and capillaries	[204]
17	Fish collagen/PCL bio-composite with covalently cross-linked chitooligosaccharides	Direct Electro-spinning	• Increased hydrophilicity, and mechanical properties of the bilayer scaffold • The porosity of the scaffold is also improved due to the electrospinning process	-	Cytocompatibility studies using human fibroblasts and keratinocytes demonstrated an effective scaffold–cell penetration and proliferation	[205]
18	Antibacterial ZnO quantum dots with PCL/collagen fibers	Direct Electro-spinning	Increased elasticity and strain, hydrophilicity, and biodegradability of the scaffolds. ZnO quantum dots provided antibacterial activity	-	Increased vascularization and promoted wound healing in early stages of wound healing	[206]
19	Ulvan–cellulose blended with polylactide and polydioxanone	Direct Electro-spinning	The fibrous scaffolds improved mechanical stability	-	In vivo angiogenesis demonstrated in rats	[207]
20	PMMA/silk fibroin	Coaxial electrospinning	Increased mechanical strength due to fiber morphology and structure Highly porous scaffolds	-	Improved adhesion and cell spreading on scaffolds in vitro	[208]
21	PCL	Melt electro-writing	Melt electro writing process enables the precise position of each individual fiber in the constructs		The precision fabrication of the fiber constructs enabled tight control of cell morphology	[209]

Abbreviations: PU, polyurethane; PGS, poly(glycerol sebacate); PCL, polycaprolactone; PLLA, poly L-lactic acid; GO, graphene oxide; PLA, poly lactic acid; PMMA, poly(methyl methacrylate); PVA, polyvinyl alcohol.

3.2. Vascular

The vascular system plays an important role in infiltrating the body's tissue to provide nutrients to the tissues. They can be classified roughly as capillaries, arterioles, veins, and arteries based on the function of these vessels. The arteries are the largest and carry oxygenated blood to the distant organs, while veins transport back the deoxygenated blood. The capillaries and arterioles act intermediates between the veins and arteries and help during the efficient transport of nutrients and waste within the organs and tissues. Depending on the function of the vessel, the shape and structure of the vessel is different. The arteries are composed of three layers of concentric tissues: the intima, media, and adventitia, each with its own unique function. The tunica intima consists

of an endothelium, a basal lamina that separates it from tunica media and an acellular endothelial layer composed of tightly bound extracellular matrix proteins, such as collage, laminin, and fibronectin. The basal lamina is elastic and composed of elastin and type IV collagen molecules. It is porous, with varying pore densities, and regulates the elasticity of the vascular wall to regulate blood pressure. Porosity also helps provide control over the diffusion of nutrients toward the surrounding tissue regions. The endothelium interacts with the blood and plays a key role in several physiological processes, such as coagulation, maintenance of vascular homeostasis, barrier, inflammation, maintenance, and modification of ECM components. The tunica media, or the middle layer, is composed of smooth muscle cells and collagen (Type I and III) in a concentric manner along the axis of the blood vessel and aid in vasodilation. The outermost layer of the blood vessel, the tunica adventitia, is composed of fibroblasts, collagen (Type I and II), mast cells, nerve endings, and different types of vasa vasorum. This layer protects the vessels from overextending or over retracting, helps in cellular trafficking and aids in cell signaling. This layer is actively involved in tissue repair and remodeling by changing the medial smooth muscle tone. Fiber-based constructs may have application in repairs to vasculature (Figure 10) [210]. Here, similarities are shown between a native artery and an implanted hyaluronic acid (HA)/collagen nanofibrous graft. In another study, a coronary artery stent that is coated with a thin electrospun nanofiber membrane has been developed for the treatment of coronary artery perforation and is being tested in human [211,212]. A summary of recent innovations relating nanofiber scaffold materials and respective mechanical, electrical and crystallinity properties studied for vascular differentiation, is listed in Table 4.

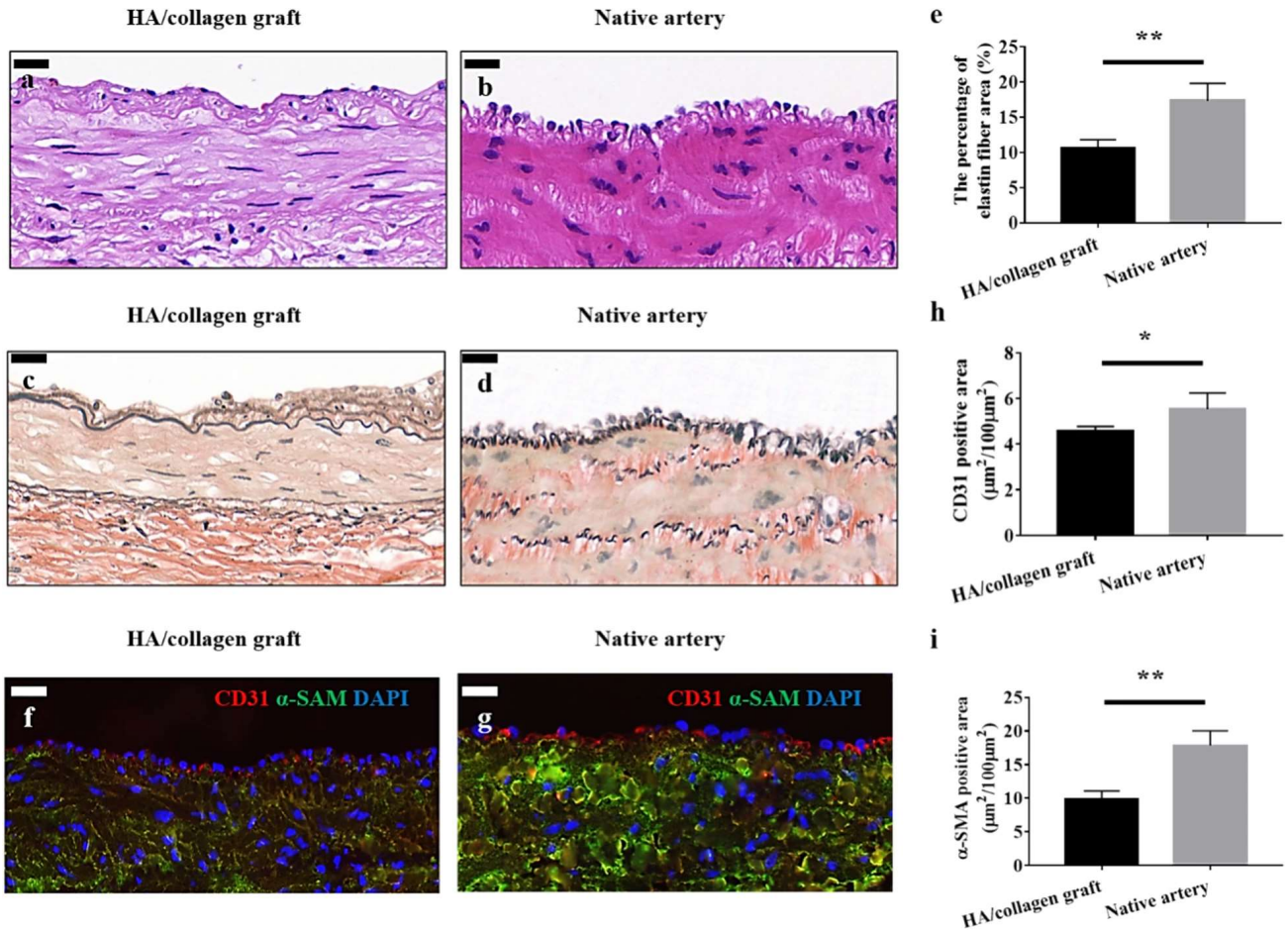

Figure 10. Vascular grafts fabricated with cellularized tubular HA/collagen nanofibrous scaffold facilitate vascular reconstruction. H&E (hemotoxylin and eosin) staining (**a**), VVG (Verhoeff–Van Gieson) staining (**c**) and fluorescent staining. (**f**)

The cross-section of a retrieved tubular HA/collagen nanofibrous graft 6 weeks after the transplant at 10× (**a**,**c**,**f**) compared with rabbit carotid artery (**b**,**d**,**g**). Scale bars, 20 μm. Fluorescence relative to vascular ECs (red), SMCs (green) and nuclei (blue). Quantification of the percentage of elastin area (**e**), CD31 (endothelial cell marker), (**h**) and α-SMA (smooth muscle actin)-positive (**i**) in the retrieved explants 6 weeks after transplant and carotid artery ($n = 3$). * $p < 0.05$, ** $p < 0.01$. Image reproduced with permission from [210].

Table 4. List of the recent innovations relating fiber-based scaffolds for engineering vascular tissue based on biophysical properties of the scaffold.

Material Used	Type of Electrospinning	Mechanical Properties	Electrical Properties	Results	Reference
PGS/PCL	Coaxial electrospinning	• Arterial vascular grafts with differences in wall stiffness were fabricated by altering the core-sheath structure • Reduced swelling of the core and eliminated stresses in sheath	-	The content of collagen varied based on stiffness, with increased smooth muscle cell and elastin content in the fibers with a thicker core	[213]
Polycarbonate–urethane	Direct electrospinning	Improved mechanical properties, including elasticity and burst pressure	-	Functionalization with fibronectin helps in fibrogenesis while with decorin repelled endothelial cells Functional endothelium was formed in dynamic conditions with fibronectin functionalization	[214]
Decellularized extracellular matrix from aorta	Direct electrospinning	• Addition of aorta ECM improved hydrophilicity • The scaffolds made from decellularized ECM had a higher mechanical strength than PCL scaffold	-	Increased cell viability and cell adherence with the use of ECM aorta	[215]
PCL cotton and membranes	Direct electrospinning	Increased porosity of fibers with comparable mechanical properties of native tissue	-	A TEVG prepared from electrospun materials when implanted in rats had similar characteristics as native vessels	[216]
PCL	Direct electrospinning	Increased anti-burst pressure and suture retention strength	-	Improved cell proliferation and viability of cells	[217]
PLGA	Direct electrospinning	Improved mechanical strength and burst pressure	-	Improved cell viability and cell proliferation with formation of tight junctions in a coculture with smooth muscle cells and endothelial cells	[218]
PCL/fibrin	Direct electrospinning	• Randomly arranged fibrous structure with high mechanical compliance • The scaffolds had controlled degradation rates	-	• Increased micro-vessel density and fewer calcifications after long-term implantation in rats • The graft induced the regeneration of arteries	[219]
Gelatin/PCL with chondroitin sulfate	Direct electrospinning	High porosity of the scaffolds with anticoagulant properties	-	Increased cell adhesion, proliferation, and increased endothelial cell responses	[220]
PU, gelatin and CNT	Direct electrospinning	• Increased hydrophilicity of scaffolds • Concentration of gelatin provided control over mechanical properties and degradation rates • Carbon nanotubes increased mechanical strength	Conductive scaffolds with electrical conductivity such as native myocardium	Increased cell adhesion and cell proliferation demonstrated in vitro, characterized by a dense layer of myocardial and endothelial cells after 7 days	[221]

Table 4. *Cont.*

Material Used	Type of Electrospinning	Mechanical Properties	Electrical Properties	Results	Reference
PCL, polydioxanone polydopamine	Co-electrospinning	• Nanotopographical cues helped in cell infiltration • The electrospinning process provided flexibility in improving mechanical properties, including tensile strength and burst pressure	-	The graft when implanted in a porcine model demonstrated good patency rates	[222]
PLA and polyethylene oxide (PEO)	Coaxial electrospinning	• PEO ratio influenced the mechanical strength and diameter of fibers • Nanoscale pores were obtained due to phase separation during the electrospinning process	-	Increased cell infiltration and growth were observed in vitro	[223]
PCL/collagen	Direct electrospinning with modified collector	Y-shaped structure was obtained by electrospinning with topographical cues along a particular direction	-	Increased directional growth and infiltration of endothelial cells	[224]
Cellulose acetate, chitosan, and PCL	Direct electrospinning with different types of collectors	Different types of topographical cues were obtained in terms of alignment of fibers and diameter	-	Aligned scaffolds interacted more with endothelial cells than platelets, they also helped in increasing proliferation and promoting angiogenesis	[225]
Poly(L-lactide-co-caprolactone)/tussah silk fibroin	Coaxial electrospinning	• Small-diameter fibers with increased hydrophilicity and mechanical properties were obtained • The core-sheath structure enhanced the axial tensile strength	-	The cell proliferation and adhesion were demonstrated in vitro	[226]
PCL/sulfonated keratin	Co-electrospinning	Fibrous scaffolds with good mechanical properties, favoring endothelial cell growth	-	• Nitric oxide generated in the presented of GSH and GSNO • The scaffolds increased endothelial cell proliferation and reduced platelet adhesion	[227]
PU and PLA	Direct electrospinning with different collectors	Different fiber orientations were fabricated	-	Some of the fiber orientations were better than the other, but a multiwalled structure was better able to mimic the rat aorta	[228]
PEGylated CdSe-ZnS quantum dots in PCL	Direct electrospinning	Narrow pore size was obtained with increased mechanical properties	-	Increased cell growth and proliferation	[229]
PET and PCL	Direct electrospinning	• The addition of PCL improved mechanical properties of the graft • Increased suture retention strength	-	Improved cell viability demonstrated in vitro	[230]
Bombyx mori-BM silk	Direct electrospinning	• The bilayer structure of the vascular graft provided interconnectivity and a porous structure • The degradation of scaffold also provided in vivo remodeling ability	-	Improved patency rate, cell infiltration, graft remodeling, neo-tissue formation	[231]
PCL and heparin conjugated 50:50 poly (l-lactide-co-ε-caprolactone) copolymer	Coaxial electrospinning	Scaffolds with different pore sizes were fabricated	-	Vascular grafts with a pore diameter smaller than 4 um had a higher patency and survival rate in vivo	[232]

Abbreviations: PU, polyurethane; PGS, poly(glycerol sebacate); PCL, polycaprolactone; PLLA, poly L-lactic acid; PLGA, poly(lactic-co-glycolic acid); PEG, polyethylene glycol; GO, graphene oxide; PLA, poly lactic acid; PEO, polyethylene oxide; PET, polyethylene terephthalate; CNT, carbon nanotubes.

3.3. Renal

The kidney serves as an important excretory organ by homeostatic regulation and purifying out waste and toxins from the blood. Apart from this key function, the kidney is also responsible for producing renin, erythropoietin, and prostaglandins. The kidney has more than a million nephrons composed of several glomerulus and tubular structures which aid in the filtration process. The glomerulus is covered by a Bowman's capsule with capillaries. These capillaries are surrounded by a negatively charged glomerular basement membrane and podocytes. The tubular structures are composed of proximal tubules, loop of Henle, distal tubules, and collecting ducts. The first stage of filtration occurs in the glomerulus, followed by secondary filtration in the tubular structures. There has been significant progress in understanding the morphogenesis of the kidney and recovery of the kidney after an injury to understand the intricate mesenchymal–epithelial transitions. Understanding the recovery process and functioning of the cells involved helps in designing efficient scaffolds for renal tissue engineering. Understanding the ECM composition of the kidney helps in better design of the scaffolds in accordance with the mechanical properties. The basement membrane of the glomerulus is controlled by the podocytes and the endothelium, and is mainly composed of structural and regulatory proteins such as collagen (I, IV and VI), laminins, and heparan sulfate proteoglycans. The mesangial cells in the glomerulus also produce ECM composed of tenascin, fibronectin and proteoglycans, which play a role in regulating the electrical charge in the glomerulus. The tubular structures have a different composition as compared to the glomerulus. The ubiquitous and heterogenous ECM composition helps in providing a complex niche for the proper functioning of the kidney. The following review by Vermue et al. (2021) analyzes some of the latest design strategies for creating an artificial proximal tubule using electrospinning [233]. A summary of recent innovations relating nanofiber scaffold materials and respective mechanical, electrical and crystallinity properties studied for renal differentiation, is listed in Table 5.

Table 5. List of the recent innovations relating fiber-based scaffolds for engineering renal tissue based on biophysical properties of the scaffold.

Material Used	Type of Electrospinning	Mechanical Properties	Electrical Properties	Results	Reference
PCL and laminin	Direct electrospinning	Scaffolds with a porous structure with a fibrous morphology were fabricated	-	Improved cell–fiber and cell–cell interaction.	[234]
PCL	Direct electrospinning	• L-DOPA and collagen were coated to increase the hydrophilicity of scaffolds • The polymer concentration played a major role in determining the mechanical properties and morphology of the scaffold, and interacted with the cells differently	-	Proximal tubules remained viable and maintained functionality for more than 3 weeks	[235]
Polyvinylidene fluoride (PVDF)	Direct electrospinning	Electrospinning with a rotating collector was used to obtain scaffold characteristics such as native renal tissue	-	Scaffolds with different pore sizes were obtained	[236]

Abbreviations: PU, polyurethane; PGS, poly(glycerol sebacate); PCL, polycaprolactone; PLLA, poly L-lactic acid; PLGA, poly(lactic-co-glycolic acid); PEG, polyethylene glycol; GO, graphene oxide; PLA, poly lactic acid; PEO, polyethylene oxide; PET, polyethylene terephthalate; CNT, carbon nanotubes.

3.4. Nerve

The restorative function in humans after injury is limited to the central nervous systems, where functional unions are formed between severed ends, while peripheral nerve tissue regeneration occurs after simple lesions. The process of peripheral nerve regeneration is complex, involving a myriad of factors. Nerve injuries can broadly be classified into neurapraxia, axonotmesis, and neurotmesis, in increasing order of injury severity. Following trauma, the neuron undergoes Wallerian degeneration, followed by several morphological and chemical changes, which can broadly be called chromatolysis. The Schwann cells are activated and macrophage recruitment to the injury site, helping in the cleanup and serving as a guide for axonal regeneration (Bands of Bunger). They also produce the required cytokines, which recruit macrophages to help with neuronal regeneration. The neuron undergoes a change from transmission mode to a growth mode, whereby the cytoskeletal proteins (slow-component b-tubulin and actin) are rapidly produced. This neuronal regeneration is different in the case of the central nervous systems (CNS), where the oligodendrocytes inhibit repair unlike the Schwann cells. Tissue engineering strategies for peripheral nerve regeneration include the use of artificial nerve guides or conduits to reconstruct the nerves when the gaps are larger than 3 cm. The Wallerian generation results in growth factors that promote regeneration. The conduits are generally placed between the two ends of the nerve to be repaired and the conduit provides guidance for the cells to bridge the gap. Some of the essential mechanical features of the tissue include electrical conductivity, protection against compression and appropriate tensile strength, which has been well reviewed [237–239]. A summary of recent innovations relating nanofiber scaffold materials and respective mechanical, electrical and crystallinity properties studied for vascular differentiation, is listed in Table 6.

Table 6. List of the recent innovations relating fiber-based scaffolds for engineering neural tissue based on biophysical properties of the scaffold.

Material Used	Type of Electrospinning	Mechanical Properties	Electrical Properties	Results	Reference
Cellulose modified with conductive polymers derivates (poly (N-(methacryl ethyl) pyrrole), poly (N-(2-hydroxyethyl) pyrrole), poly (3-(Ethoxycarbonyl) thiophene), and poly (3-thiophenethanol)	Direct electrospinning	The composite fibers had high hydrophilicity, surface roughness, and porosity	Electrically conductive scaffolds that benefitted nerve growth were obtained	Increased cell adhesion and growth with clear-cell morphology were observed when PC12 cells were seeded on scaffolds	[240]
PCL/gelatin with melatonin	Direct electrospinning	The fibers had higher hydrophilicity and surface properties	-	The use of melatonin helped in the growth and proliferation of nerve cells in vitro	[241]
Silk fibroin/poly(l-lactic acid-co-ε-caprolactone)	Direct electrospinning	A 3D scaffold with higher porosity, mechanical strength with adequate strength for suture implantation		The prevascularization of the scaffolds aided in nerve functional recovery	[242]
Poly(lactide-co-trimethylene carbonate) based on lactic acid and trimethylene carbonate	Direct electrospinning	A shape memory polymer was used to fabricate conduits with high porosity and mechanical strength by combining aligned fiber mat and random fiber mat to form a multichannel	-	The structure provides uniform loading of cells and topographical cues for axon elongation and nerve regeneration	[243]

Table 6. *Cont.*

Material Used	Type of Electrospinning	Mechanical Properties	Electrical Properties	Results	Reference
Pure porcine decellularized nerve matrix and proanthocyanidins	Direct electrospinning	The use of proanthocyanidins increased the mechanical properties of the fibers.	Conduction velocities of 8.86 ± 3.57 m/s were obtained	Studies performed on rabbits demonstrated the elongation of axon and myelination using the scaffolds	[244]
PCL conduit filled with collagen–hyaluronic acid	Direct electrospinning	• The presence of HA helped in controlling the degradation rates • The scaffolds were porous and had good mechanical strength	-	The scaffolds promoted Schwann cell regeneration and axon growth	[245]
PLGA	Direct electrospinning	• Different ratios of polylactic and polyglycolic acid were used to obtain scaffolds with layers • The layers had different degradation rates and mechanical properties	-	The rat Schwann cells exhibited favorable growth on the scaffolds in vitro	[246]

Abbreviations: PCL, polycaprolactone; HA, hyaluronic acid; PLGA, poly(lactic-co-glycolic acid).

3.5. Cardiac Tissue

The heart is a marvel of engineering and is structurally and functionally a complex pump that circulates blood within the body and is hence vital to survival. The heart is composed of cardiomyocytes and fibroblasts with a collagen ECM. The muscles in the heart use a lot of oxygen and are supported by vasculature. The heart tissue is electrically conductive and uses this to control the contraction of muscles to pump blood. Failure of the heart is beyond repair and is one of the leading causes of death in the USA. Myocardial infarction of the heart muscles leads to the formation of scar tissues due to the action of macrophages, endothelial cells, and fibroblasts that are recruited to the site through inflammatory signals. The presence of scar tissue in turn reduces the mechanical capability of the heart to pump blood, which ultimately leads to total heart failure. The reconstruction of heart tissue using cardiac patches is currently being researched to aid in cardiac regeneration and prevention of scar tissue formation. Apart from challenges in the choice of cells and type of grafts, the mechanical and electrical properties are an important factor. The graft or patch needs to work synchronously with the existing tissue in propagating the signal. This includes mimicking the electrical resistance of the tissue or having similar mechanical properties (Figure 11).

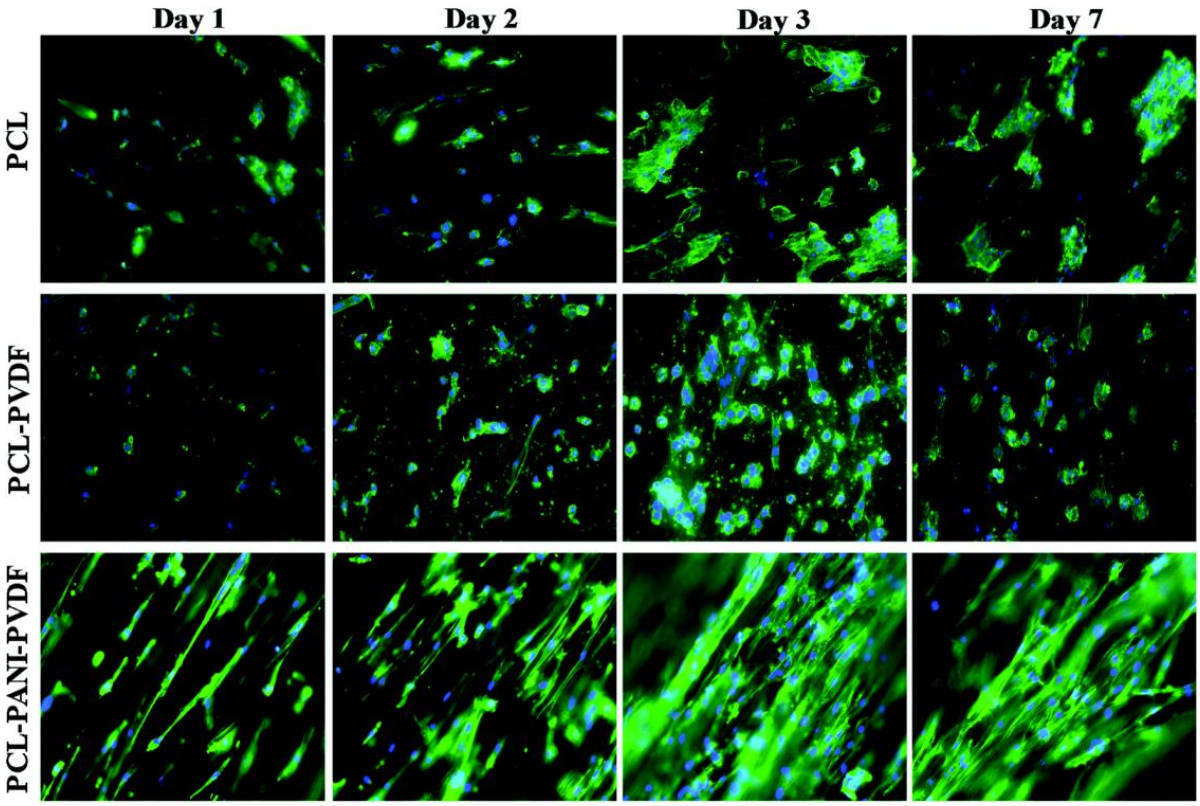

Figure 11. Comparison of rat cardiomyoblast (H9c2) cells on PCL, PCL-PANI, and PCL-PANI-PVDF scaffolds on different days. Blue: DAPI nuclei stain; green: Alexa fluor® 488 Phalloidin for F-actin filaments. Image adapted from [247].

Roshanbinfar et al. (2020) reported the use of electrospun nanofiber scaffolds, using direct electrospinning for cardiac tissue engineering. They used collagen (9.89%), hyaluronic acid (1.1%), and polyaniline (PANi, 1.34%). The cardiomyocytes seeded on scaffolds exhibited longer contraction times, improved electrical coupling with lower cytotoxicity, and enhanced cell attachment and cardiac function. The polymer composition used gave rise to electrical and mechanical properties similar to the native myocardium. The same study compared outcomes with combinations of different polymers, including collagen, hyaluronic acid and four different concentrations of PANi [248].

3.6. Retinal Pigment Epithelium

The retinal pigment epithelium (RPE) is a layer of cells in the eye that supports photoreceptors that are responsible for sensing light. In vision disorders such as age-related macular degeneration, the RPE can degrade and cause a loss of photoreceptor function and vision. A number of tissue engineering approaches are being advanced to repair the RPE [249,250]. Some of these strategies entail growing the RPE in a lab on a fiber-based scaffold and then implanting the cell–scaffold construct into the eye [251]. Several studies have demonstrated that the electrospun fibers mimic the structure of the native Bruch's membrane upon which the RPE resides in vivo, and that the RPE cultured on electrospun fibers retained many of the properties of native the RPE [252–258]. Liu et al. (2014) found that the in vitro culture of RPE on fiber-based scaffolds led to a deeper pigmentation and more uniform hexagonal tight junctions, and that the native RPE migrated onto the scaffolds following implantation [259]. In a study of rodent and pig models that had laser-induced RPE injuries, the induced pluripotent stem-cell-derived RPE that was generated on an electrospun fiber patch was implanted and able to improve RPE functionality as compared to scaffold-free cell suspensions [260].

4. Challenges for Fiber-Based Scaffolds

Several challenges exist for advancing fiber-based scaffolds for tissue engineering applications. Herein, the focus has been on cell responses to fibers. However, in vitro cell culture responses and responses following human implantation do not have a 1:1 correlation. Cell differentiation on a fiber scaffold in vitro does not mean that an implanted fiber scaffold will induce tissue regeneration in humans. It is important to improve the quality of in vitro models to better mimic human physiological response. Next, environmental control is important for fiber processing and manufacturing, but it is hard to achieve. Temperature, humidity, particulates, and solvent build up in the atmosphere during electrospinning, and can have a large impact on fiber properties. It is much more expensive and difficult to establish environmental control than it is to set up an electrospinning system. There are no clear mechanisms to establish reliable environmental controls to enable consistent fiber manufacturing, and each lab and organization must develop their own mechanisms to suit their budget and capability, largely through trial and error. Fully understanding the environmental impact on nanofiber properties will be essential for the reproducibility and scale-up of nanofiber technologies for tissue engineering. Another issue is profitability. Often, the required implant for each patient may be tiny, with dimensions such as 1 mm $\times$ 2 mm. A large-scale manufacturer may be able to make 1-m-wide rolls of fiber scaffolds, providing enough scaffold material for tens of thousands of patients in a day. In addition, the amount of raw polymer material required to treat one patient may be a few milligrams, with a value of only a few dollars. Nevertheless, the raw material provider becomes exposed to significant medical liability by allowing their materials to be used to treat humans. Thus, supplying a scaffold for humans use may have a high risk with a small profit margin, which presents a challenge to investors that want to commercialize fiber-scaffold-based therapies.

5. Conclusions

The vast body of research available on nanofiber scaffolds reiterates the wide range of tunability, both in terms of materials that can be used and structures that can be created. Different tissues rely on different cues: physical, chemical, and biological, that guide cell growth, migration, and differentiation. Nanofiber scaffolds have several key advantages, and have carved out a niche in the field of engineered tissues and regenerative medicine. Several key aspects, such as mechanical properties, pore size, porosity, crystallinity, alignment, and fiber diameter, support different requirements of the cells. Despite the widespread use of nanofiber scaffolds for 3D cultures and tissue engineering, there remains a lack of industry standard for the manufacturing, quality control, and guidelines for the application of specific scaffolds for specific tissues or cells. Thus, there is a huge unmet need in the standardization of 3D tissue culture approaches using nanofiber scaffolds that may lead to conflicting outcomes. While the majority of the work has been focused on identifying materials and scaffold properties, efforts to better understand the biomechanical interactions will establish scaffold parameters needed for specific tissues. For example, further investigation into how nanofiber alignment affects porosity, and how this in turn affects tissue regeneration, is needed. Complex tissue systems with multilayered structures and vasculature will benefit from further exploring polymer blends, controlling morphology and nanotopography, and mimicking the physiological, biological, and mechanical properties of the different layers of the tissue. Consideration should be given to improving cost and time, and achieving the scale-up of manufacturing. In addition, investigating a combination of electrospun scaffolds with other techniques, such as bioprinting or hybrid systems combining hydrogels and scaffolds, should be further explored. These have the potential to improve in vitro outcomes and may prove successful in vivo. Nanofiber scaffolds have several advantages that make them a viable option for tissue regeneration applications. Combining this technology with others may prove to be the final step in realizing tissue regeneration through tissue engineering.

Author Contributions: Conceptualization, J.D., S.N.H., S.F. and S.R.; Methodology, J.D., S.N.H., S.F. and S.R.; Validation, S.N.H., S.F., C.G.S.J. and S.R.; Writing-original draft preparation, J.D., S.N.H. and S.R.; Writing-review and editing, J.D., S.N.H., S.F., S.R. and C.G.S.J.; Project Administration, J.D., S.N.H. and S.R.; Supervision, S.N.H., S.F., S.R. and C.G.S.J. All authors have read and agreed to the published version of the manuscript.

Funding: This research received no external funding.

Data Availability Statement: No new data were created or analyzed in this study. Data sharing is not applicable to this article.

Conflicts of Interest: The authors declare no conflict of interest.

References

1. Na, S.; Collin, O.; Chowdhury, F.; Tay, B.; Ouyang, M.; Wang, Y.; Wang, N. Rapid signal transduction in living cells is a unique feature of mechanotransduction. *Proc. Natl. Acad. Sci. USA* **2008**, *105*, 6626–6631. [CrossRef]
2. Dessauge, F.; Schleder, C.; Perruchot, M.-H.; Rouger, K. 3D in vitro models of skeletal muscle: Myopshere, myobundle and bioprinted muscle construct. *Vet. Res.* **2021**, *52*, 72. [CrossRef] [PubMed]
3. Cha, S.H.; Lee, H.J.; Koh, W.G. Study of myoblast differentiation using multi-dimensional scaffolds consisting of nano and micropatterns. *Biomater. Res.* **2017**, *21*, 1. [CrossRef]
4. Nguyen-Truong, M.; Li, Y.V.; Wang, Z. Mechanical Considerations of Electrospun Scaffolds for Myocardial Tissue and Regenerative Engineering. *Bioengineering* **2020**, *7*, 122. [CrossRef] [PubMed]
5. Ding, S.; Kingshott, P.; Thissen, H.; Pera, M.; Wang, P.-Y. Modulation of human mesenchymal and pluripotent stem cell behavior using biophysical and biochemical cues: A review. *Biotechnol. Bioeng.* **2017**, *114*, 260–280. [CrossRef]
6. Liu, H.; Paul, C.; Xu, M. Optimal Environmental Stiffness for Stem Cell Mediated Ischemic Myocardium Repair. In *Adult Stem Cells*; Springer: New York, NY, USA, 2017; pp. 293–304.
7. Saxena, N.; Mogha, P.; Dash, S.; Majumder, A.; Jadhav, S.; Sen, S. Matrix elasticity regulates mesenchymal stem cell chemotaxis. *J. Cell Sci.* **2018**, *131*, jcs211391. [CrossRef]
8. Wang, M.; Cheng, B.; Yang, Y.; Liu, H.; Huang, G.; Han, L.; Li, F.; Xu, F. Microchannel Stiffness and Confinement Jointly Induce the Mesenchymal-Amoeboid Transition of Cancer Cell Migration. *Nano Lett.* **2019**, *19*, 5949–5958. [CrossRef] [PubMed]
9. Pauly, H.M.; Kelly, D.J.; Popat, K.C.; Trujillo, N.A.; Dunne, N.J.; McCarthy, H.O.; Donahue, T.L.H. Mechanical properties and cellular response of novel electrospun nanofibers for ligament tissue engineering: Effects of orientation and geometry. *J. Mech. Behav. Biomed Mater.* **2016**, *61*, 258–270. [CrossRef]
10. Choi, Y.S.; Vincent, L.G.; Lee, A.R.; Kretchmer, K.C.; Chirasatitsin, S.; Dobke, M.K.; Engler, A.J. The alignment and fusion assembly of adipose-derived stem cells on mechanically patterned matrices. *Biomaterials* **2012**, *33*, 6943–6951. [CrossRef] [PubMed]
11. Jagiełło, A.; Hu, Q.; Castillo, U.; Botvinick, E. Patterned photocrosslinking to establish stiffness anisotropies in fibrous 3D hydrogels. *Acta Biomater.* **2022**, *141*, 39–47. [CrossRef]
12. Yang, C.-Y.; Huang, W.-Y.; Chen, L.-H.; Liang, N.-W.; Wang, H.-C.; Lu, J.; Wang, X.; Wang, T.-W. Neural tissue engineering: The influence of scaffold surface topography and extracellular matrix microenvironment. *J. Mater. Chem. B* **2021**, *9*, 567–584. [CrossRef] [PubMed]
13. Lee, C.H.; Shin, H.J.; Cho, I.H.; Kang, Y.-M.; Kim, I.A.; Park, K.-D.; Shin, J.-W. Nanofiber alignment and direction of mechanical strain affect the ECM production of human ACL fibroblast. *Biomaterials* **2005**, *26*, 1261–1270. [CrossRef] [PubMed]
14. Forte, G.; Pagliari, S.; Ebara, M.; Uto, K.; Van Tam, J.K.; Romanazzo, S.; Escobedo-Lucea, C.; Romano, E.; Di Nardo, P.; Traversa, E.; et al. Substrate stiffness modulates gene expression and phenotype in neonatal cardiomyocytes in vitro. *Tissue Eng. Part A* **2012**, *18*, 1837–1848. [CrossRef] [PubMed]
15. *ASTM F3510-21*; Standard Guide for Characterizing Fiber-Based Constructs for TissueEngineered Medical Products. ASTM International: West Conshohocken, PA, USA, 2021.
16. Roldán, G.J.C.; Martínez, Y.Q.; Gómez, L.M.A.; Vinasco, L.F.R.; Palacio, L.M.H. Influence of the molecular weight of polymer, solvents and operational condition in the electrospinning of polycaprolactone. *Rev. Fac. Ing. Univ. Antioq.* **2017**, *2017*, 35–45. [CrossRef]
17. Ameer, J.M.; Pr, A.K.; Kasoju, N. Strategies to Tune Electrospun Scaffold Porosity for Effective Cell Response in Tissue Engineering. *J. Funct. Biomater.* **2019**, *10*, 30. [CrossRef]
18. Harley, B.A.; Kim, H.-D.; Zaman, M.H.; Yannas, I.V.; Lauffenburger, D.A.; Gibson, L.J. Microarchitecture of three-dimensional scaffolds influences cell migration behavior via junction interactions. *Biophys. J.* **2008**, *95*, 4013–4024. [CrossRef]
19. Vagaská, B.; Bačáková, L.; Filová, E.; Balík, K. Osteogenic Cells on Bio-Inspired Materials for Bone Tissue Engineering. *Physiol. Res.* **2010**, *59*, 309–322. [CrossRef]
20. Filippi, M.; Born, G.; Chaaban, M.; Scherberich, A. Natural Polymeric Scaffolds in Bone Regeneration. *Front. Bioeng. Biotechnol.* **2020**, *8*, 474. [CrossRef]
21. Smith, I.O.; Liu, X.H.; Smith, L.A.; Ma, P.X. Nanostructured polymer scaffolds for tissue engineering and regenerative medicine. *Wiley Interdiscip. Rev. Nanomed. Nanobiotechnol.* **2009**, *1*, 226–236. [CrossRef]

22. Murphy, C.M.; Haugh, M.G.; O'Brien, F.J. The effect of mean pore size on cell attachment, proliferation and migration in collagen-glycosaminoglycan scaffolds for bone tissue engineering. *Biomaterials* **2010**, *31*, 461–466. [CrossRef]
23. Chen, X.; Fu, X.; Shi, J.-G.; Wang, H. Regulation of the osteogenesis of pre-osteoblasts by spatial arrangement of electrospun nanofibers in two- and three-dimensional environments. *Nanomed. Nanotechnol. Biol. Med.* **2013**, *9*, 1283–1292. [CrossRef]
24. Bružauskaitė, I.; Bironaitė, D.; Bagdonas, E.; Bernotienė, E. Scaffolds and cells for tissue regeneration: Different scaffold pore sizes-different cell effects. *Cytotechnology* **2016**, *68*, 355–369. [CrossRef] [PubMed]
25. Nitti, P.; Gallo, N.; Natta, L.; Scalera, F.; Palazzo, B.; Sannino, A.; Gervaso, F. Influence of Nanofiber Orientation on Morphological and Mechanical Properties of Electrospun Chitosan Mats. *J. Healthc. Eng.* **2018**, *2018*, 3651480. [CrossRef] [PubMed]
26. Li, W.-J.; Mauck, R.L.; Cooper, J.A.; Yuan, X.; Tuan, R.S. Engineering controllable anisotropy in electrospun biodegradable nanofibrous scaffolds for musculoskeletal tissue engineering. *J. Biomech.* **2007**, *40*, 1686–1693. [CrossRef]
27. Patel, K.H.; Dunn, A.J.; Talovic, M.; Haas, G.J.; Marcinczyk, M.; Elmashhady, H.; Kalaf, E.G.; Sell, S.A.; Garg, K. Aligned nanofibers of decellularized muscle ECM support myogenic activity in primary satellite cells in vitro. *Biomed. Mater.* **2019**, *14*, 035010. [CrossRef] [PubMed]
28. Patel, K.H.; Talovic, M.; Dunn, A.J.; Patel, A.; Vendrell, S.; Schwartz, M.; Garg, K. Aligned nanofibers of decellularized muscle extracellular matrix for volumetric muscle loss. *J. Biomed. Mater. Res. Part B Appl. Biomater.* **2020**, *108*, 2528–2537. [CrossRef] [PubMed]
29. Kawano, T.; Sato, M.; Yabu, H.; Shimomura, M. Honeycomb-shaped surface topography induces differentiation of human mesenchymal stem cells (hMSCs): Uniform porous polymer scaffolds prepared by the breath figure technique. *Biomater. Sci.* **2014**, *2*, 52–56. [CrossRef]
30. Narayanan, N.; Jiang, C.; Wang, C.; Uzunalli, G.; Whittern, N.; Chen, D.; Jones, O.G.; Kuang, S.; Deng, M. Harnessing Fiber Diameter-Dependent Effects of Myoblasts Toward Biomimetic Scaffold-Based Skeletal Muscle Regeneration. *Front. Bioeng. Biotechnol.* **2020**, *8*, 203. [CrossRef]
31. Kroehne, V.; Heschel, I.; Schügner, F.; Lasrich, D.; Bartsch, J.W.; Jockusch, H. Use of a novel collagen matrix with oriented pore structure for muscle cell differentiation in cell culture and in grafts. *J. Cell. Mol. Med.* **2008**, *12*, 1640–1648. [CrossRef]
32. Lowery, J.L.; Datta, N.; Rutledge, G.C. Effect of fiber diameter, pore size and seeding method on growth of human dermal fibroblasts in electrospun poly(ε-caprolactone) fibrous mats. *Biomaterials* **2010**, *31*, 491–504. [CrossRef]
33. Nguyen, J.H.; Chung, J.D.; Lynch, G.S.; Ryall, J.G. The Microenvironment Is a Critical Regulator of Muscle Stem Cell Activation and Proliferation. *Front. Cell Dev. Biol.* **2019**, *7*, 254. [CrossRef] [PubMed]
34. Perez-Puyana, V.; Wieringa, P.; Yuste, Y.; de la Portilla, F.; Guererro, A.; Romero, A.; Moroni, L. Fabrication of hybrid scaffolds obtained from combinations of PCL with gelatin or collagen via electrospinning for skeletal muscle tissue engineering. *J. Biomed Mater. Res. A* **2021**, *109*, 1600–1612. [CrossRef] [PubMed]
35. Cooper, A.; Jana, S.; Bhattarai, N.; Zhang, M. Aligned chitosan-based nanofibers for enhanced myogenesis. *J. Mater. Chem.* **2010**, *20*, 8904. [CrossRef]
36. Badami, A.S.; Kreke, M.R.; Thompson, M.S.; Riffle, J.S.; Goldstein, A.S. Effect of fiber diameter on spreading, proliferation, and differentiation of osteoblastic cells on electrospun poly(lactic acid) substrates. *Biomaterials* **2006**, *27*, 596–606. [CrossRef]
37. Ma, B.; Xie, J.; Jiang, J.; Shuler, F.D.; E Bartlett, D. Rational design of nanofiber scaffolds for orthopedic tissue repair and regeneration. *Nanomedicine* **2013**, *8*, 1459–1481. [CrossRef]
38. Bloise, N.; Berardi, E.; Gualandi, C.; Zaghi, E.; Gigli, M.; Duelen, R.; Ceccarelli, G.; Cortesi, E.E.; Costamagna, D.; Bruni, G.; et al. Ether-Oxygen Containing Electrospun Microfibrous and Sub-Microfibrous Scaffolds Based on Poly(butylene 1,4-cyclohexanedicarboxylate) for Skeletal Muscle Tissue Engineering. *Int. J. Mol. Sci.* **2018**, *19*, 3212. [CrossRef]
39. Jo, S.B.; Erdenebileg, U.; Dashnyam, K.; Jin, G.-Z.; Cha, J.-R.; El-Fiqi, A.; Knowles, J.C.; Patel, K.D.; Lee, H.-H.; Lee, J.-H.; et al. Nano-graphene oxide/polyurethane nanofibers: Mechanically flexible and myogenic stimulating matrix for skeletal tissue engineering. *J. Tissue Eng.* **2020**, *11*, 2041731419900424. [CrossRef]
40. Saburi, E.; Islami, M.; Hosseinzadeh, S.; Moghadam, A.S.; Mansour, R.N.; Azadian, E.; Joneidi, Z.; Nikpoor, A.R.; Ghadiani, M.H.; Khodaii, Z.; et al. In vitro osteogenic differentiation potential of the human induced pluripotent stem cells augments when grown on Graphene oxide-modified nanofibers. *Gene* **2019**, *696*, 72–79. [CrossRef]
41. Gaharwar, A.K.; Nikkhah, M.; Sant, S.; Khademhosseini, A. Anisotropic poly (glycerol sebacate)-poly (ϵ-caprolactone) electrospun fibers promote endothelial cell guidance. *Biofabrication* **2014**, *7*, 015001. [CrossRef]
42. Shi, D.; Mi, G.; Wang, M.; Webster, T.J. In vitro and ex vivo systems at the forefront of infection modeling and drug discovery. *Biomaterials* **2019**, *198*, 228–249. [CrossRef]
43. Sarkar, K.; Gomez, C.; Zambrano, S.; Ramirez, M.; de Hoyos, E.; Vasquez, H.; Lozano, K. Electrospinning to Forcespinning (TM). *Mater. Today* **2010**, *13*, 12–14. [CrossRef]
44. Gajjar, C.R.; Stallrich, J.W.; Pasquinelli, M.A.; King, M.W. Process–Property Relationships for Melt-Spun Poly(lactic acid) Yarn. *ACS Omega* **2021**, *6*, 15920–15928. [CrossRef] [PubMed]
45. Dorthé, E.W.; Williams, A.B.; Grogan, S.P.; D'lima, D.D. Pneumatospinning Biomimetic Scaffolds for Meniscus Tissue Engineering. *Front. Bioeng. Biotechnol.* **2022**, *10*, 810705. [CrossRef] [PubMed]
46. Song, J.; Li, Z.; Wu, H. Blowspinning: A New Choice for Nanofibers. *ACS Appl. Mater. Interfaces* **2020**, *12*, 33447–33464. [CrossRef]
47. Brown, T.D.; Slotosch, A.; Thibaudeau, L.; Taubenberger, A.; Loessner, D.; Vaquette, C.; Dalton, P.D.; Hutmacher, D.W. Design and Fabrication of Tubular Scaffolds via Direct Writing in a Melt Electrospinning Mode. *Biointerphases* **2012**, *7*, 13. [CrossRef]

48. Breitenbach, J. Melt extrusion: From process to drug delivery technology. *Eur. J. Pharm. Biopharm.* **2002**, *54*, 107–117. [CrossRef]
49. Lavin, D.M.; Harrison, M.W.; Tee, L.Y.; Wei, K.A.; Mathiowitz, E. A novel wet extrusion technique to fabricate self-assembled microfiber scaffolds for controlled drug delivery. *J. Biomed. Mater. Res. A* **2012**, *100*, 2793–2802. [CrossRef]
50. Mohd Pu'Ad, N.A.S.; Haq, R.H.A.; Noh, H.M.; Abdullah, H.Z.; Idris, M.I.; Lee, T.C. Review on the fabrication of fused deposition modelling (FDM) composite filament for biomedical applications. *Mater. Today Proc.* **2020**, *29*, 228–232. [CrossRef]
51. Martella, D.; Parmeggiani, C. Advances in Cell Scaffolds for Tissue Engineering: The Value of Liquid Crystalline Elastomers. *Chem. A Eur. J.* **2018**, *24*, 12206–12220. [CrossRef]
52. Cheng, X.; Gurkan, U.A.; Dehen, C.J.; Tate, M.P.; Hillhouse, H.W.; Simpson, G.J.; Akkus, O. An electrochemical fabrication process for the assembly of anisotropically oriented collagen bundles. *Biomaterials* **2008**, *29*, 3278–3288. [CrossRef]
53. Yadavalli, N.S.; Asheghali, D.; Tokarev, A.; Zhang, W.; Xie, J.; Minko, S. Gravity Drawing of Micro- and Nanofibers for Additive Manufacturing of Well-Organized 3D-Nanostructured Scaffolds. *Small* **2020**, *16*, 1907422. [CrossRef]
54. Wu, S.; Wang, Y.; Streubel, P.N.; Duan, B. Living nanofiber yarn-based woven biotextiles for tendon tissue engineering using cell tri-culture and mechanical stimulation. *Acta Biomater.* **2017**, *62*, 102–115. [CrossRef]
55. Wu, S.; Duan, B.; Liu, P.; Zhang, C.; Qin, X.; Butcher, J.T. Fabrication of Aligned Nanofiber Polymer Yarn Networks for Anisotropic Soft Tissue Scaffolds. *Acs Appl. Mater. Interfaces* **2016**, *8*, 16950–16960. [CrossRef]
56. Wu, T.; Zhang, J.; Wang, Y.; Li, D.; Sun, B.; El-Hamshary, H.; Yin, M.; Mo, X. Fabrication and preliminary study of a biomimetic tri-layer tubular graft based on fibers and fiber yarns for vascular tissue engineering. *Mater. Sci. Eng. C-Mater. Biol. Appl.* **2018**, *82*, 121–129. [CrossRef] [PubMed]
57. Chartrain, N.A.; Williams, C.B.; Whittington, A.R. A review on fabricating tissue scaffolds using vat photopolymerization. *Acta Biomater.* **2018**, *74*, 90–111. [CrossRef] [PubMed]
58. Ahn, J.-H.; Kim, J.; Han, G.; Kim, D.; Cheon, K.-H.; Lee, H.; Kim, H.-E.; Kim, Y.-J.; Jang, T.-S.; Jung, H.-D. 3D-printed biodegradable composite scaffolds with significantly enhanced mechanical properties via the combination of binder jetting and capillary rise infiltration process. *Addit. Manuf.* **2021**, *41*, 101988. [CrossRef]
59. Kim, C.K.; Jeong, J.I.; Choi, S.G.; Kim, J.H.; Cho, Y.T. High-throughput directed energy deposition process with an optimized scanning nozzle. *J. Mater. Process. Technol.* **2021**, *295*, 117165. [CrossRef]
60. Zhu, J.L.; Kaufman, L.J. Collagen I Self-Assembly: Revealing the Developing Structures that Generate Turbidity. *Biophys. J.* **2014**, *106*, 1822–1831. [CrossRef]
61. FDA. Guidance for the Preparation of a Premarket Notification Application for a Surgical Mesh. In *Guidance for Industry and/or for FDA Reviewers/Staff and/or Compliance*; Food and Drug Administration, U.S. Department of Health and Human Services, Center for Devices and Radiological Health, Eds.; FDA: Silver Spring, MD, USA, 1999.
62. Mao, N.; Russell, S.J.; Pourdeyhimi, B. Characterisation, testing, and modelling of nonwoven fabrics. In *Handbook of Nonwovens*; Elsevier: Amsterdam, The Netherlands, 2022; pp. 509–626.
63. Tucker, N.; Stanger, J.J.; Staiger, M.P.; Razzaq, H.; Hofman, K. The history of the science and technology of electrospinning from 1600 to 1995. *J. Eng. Fibers Fabr.* **2012**, *7* (Suppl. S2), 155892501200702S10. [CrossRef]
64. Bhardwaj, N.; Kundu, S.C. Electrospinning: A fascinating fiber fabrication technique. *Biotechnol. Adv.* **2010**, *28*, 325–347. [CrossRef]
65. Teo, W.E.; Ramakrishna, S. A review on electrospinning design and nanofibre assemblies. *Nanotechnology* **2006**, *17*, R89. [CrossRef]
66. Subbiah, T.; Bhat, G.S.; Tock, R.W.; Parameswaran, S.; Ramkumar, S.S. Electrospinning of nanofibers. *J. Appl. Polym. Sci.* **2005**, *96*, 557–569. [CrossRef]
67. Bognitzki, M.; Czado, W.; Frese, T.; Schaper, A.; Hellwig, M.; Steinhart, M.; Greiner, A.; Wendorff, J.H. Nanostructured fibers via electrospinning. *Adv. Mater.* **2001**, *13*, 70–72. [CrossRef]
68. Li, D.; Xia, Y. Electrospinning of nanofibers: Reinventing the wheel? *Adv. Mater.* **2004**, *16*, 1151–1170. [CrossRef]
69. Tong, H.-W.; Wang, M. Electrospinning of fibrous polymer scaffolds using positive voltage or negative voltage: A comparative study. *Biomed. Mater.* **2010**, *5*, 054110. [CrossRef]
70. Doshi, J.; Reneker, D.H. Electrospinning process and applications of electrospun fibers. *J. Electrost.* **1995**, *35*, 151–160. [CrossRef]
71. Mailley, D.; Hebraud, A.; Schlatter, G. A review on the impact of humidity during electrospinning: From the nanofiber structure engineering to the applications. *Macromol. Mater. Eng.* **2021**, *306*, 2100115. [CrossRef]
72. Pelipenko, J.; Kristl, J.; Janković, B.; Baumgartner, S.; Kocbek, P. The impact of relative humidity during electrospinning on the morphology and mechanical properties of nanofibers. *Int. J. Pharm.* **2013**, *456*, 125–134. [CrossRef] [PubMed]
73. Cai, Y.; Gevelber, M. The effect of relative humidity and evaporation rate on electrospinning: Fiber diameter and measurement for control implications. *J. Mater. Sci.* **2013**, *48*, 7812–7826. [CrossRef]
74. Kumar, P. Effect of Colletor on Electrospinning to Fabricate Aligned Nano Fiber. Bachelor's Thesis, National Institute of Technology, Rourkela, India, 2012.
75. Hohman, M.M.; Shin, M.; Rutledge, G.; Brenner, M.P. Electrospinning and electrically forced jets. II. Applications. *Phys. Fluids* **2001**, *13*, 2221–2236. [CrossRef]
76. Rosell-Llompart, J.; Grifoll, J.; Loscertales, I.G. Electrosprays in the cone-jet mode: From Taylor cone formation to spray development. *J. Aerosol Sci.* **2018**, *125*, 2–31. [CrossRef]
77. Yarin, A.L.; Koombhongse, S.; Reneker, D.H. Taylor cone and jetting from liquid droplets in electrospinning of nanofibers. *J. Appl. Phys.* **2001**, *90*, 4836–4846. [CrossRef]

78. Stanger, J.; Tucker, N.; Kirwan, K.; Staiger, M. Effect of charge density on the Taylor cone in electrospinning. *Int. J. Mod. Phys. B* **2009**, *23*, 1956–1961. [CrossRef]
79. Vaseashta, A. Controlled formation of multiple Taylor cones in electrospinning process. *Appl. Phys. Lett.* **2007**, *90*, 093115. [CrossRef]
80. Li, Z.; Wang, C. Effects of working parameters on electrospinning. In *One-Dimensional Nanostructures*; Springer: Berlin/Heidelberg, Germany, 2013; pp. 15–28.
81. Li, Y.; Zhu, J.; Cheng, H.; Li, G.; Cho, H.; Jiang, M.; Gao, Q.; Zhang, X. Developments of advanced electrospinning techniques: A critical review. *Adv. Mater. Technol.* **2021**, *6*, 2100410. [CrossRef]
82. Nagam Hanumantharao, S.; Que, C.; Rao, S. Self-assembly of 3D nanostructures in electrospun polycaprolactone-polyaniline fibers and their application as scaffolds for tissue engineering. *Materialia* **2019**, *6*, 100296. [CrossRef]
83. Park, S.M.; Eom, S.; Kim, W.; Kim, D.S. Role of grounded liquid collectors in precise patterning of electrospun nanofiber mats. *Langmuir* **2018**, *34*, 284–290. [CrossRef]
84. Li, S.; Lee, B.K. Electrospinning of circumferentially aligned polymer nanofibers floating on rotating water collector. *J. Appl. Polym. Sci.* **2020**, *137*, 48759. [CrossRef]
85. Zhang, D.; Chang, J. Electrospinning of three-dimensional nanofibrous tubes with controllable architectures. *Nano Lett.* **2008**, *8*, 3283–3287. [CrossRef] [PubMed]
86. Zhang, D.; Chang, J. Patterning of electrospun fibers using electroconductive templates. *Adv. Mater.* **2007**, *19*, 3664–3667. [CrossRef]
87. Lei, T.; Xu, Z.; Cai, X.; Xu, L.; Sun, D. New insight into gap electrospinning: Toward meter-long aligned nanofibers. *Langmuir* **2018**, *34*, 13788–13793. [CrossRef]
88. Liu, Y.; Zhang, X.; Xia, Y.; Yang, H. Magnetic-field-assisted electrospinning of aligned straight and wavy polymeric nanofibers. *Adv. Mater.* **2010**, *22*, 2454–2457. [CrossRef]
89. Dalton, P.D.; Klee, D.; Möller, M. Electrospinning with dual collection rings. *Polymer* **2005**, *46*, 611–614. [CrossRef]
90. Yoon, J.; Yang, H.-S.; Lee, B.-S.; Yu, W.-R. Recent progress in coaxial electrospinning: New parameters, various structures, and wide applications. *Adv. Mater.* **2018**, *30*, 1704765. [CrossRef]
91. Khalf, A.; Madihally, S.V. Recent advances in multiaxial electrospinning for drug delivery. *Eur. J. Pharm. Biopharm.* **2017**, *112*, 1–17. [CrossRef]
92. Bazilevsky, A.V.; Yarin, A.L.; Megaridis, C.M. Co-electrospinning of core- shell fibers using a single-nozzle technique. *Langmuir* **2007**, *23*, 2311–2314. [CrossRef] [PubMed]
93. Wannatong, L.; Sirivat, A.; Supaphol, P. Effects of solvents on electrospun polymeric fibers: Preliminary study on polystyrene. *Polym. Int.* **2004**, *53*, 1851–1859. [CrossRef]
94. Luo, C.; Nangrejo, M.; Edirisinghe, M. A novel method of selecting solvents for polymer electrospinning. *Polymer* **2010**, *51*, 1654–1662. [CrossRef]
95. Hodge, J.; Quint, C. The improvement of cell infiltration in an electrospun scaffold with multiple synthetic biodegradable polymers using sacrificial PEO microparticles. *J. Biomed. Mater. Res. Part A* **2019**, *107*, 1954–1964. [CrossRef]
96. Dang, J.M.; Leong, K.W. Natural polymers for gene delivery and tissue engineering. *Adv. Drug Deliv. Rev.* **2006**, *58*, 487–499. [CrossRef] [PubMed]
97. Sell, S.A.; Wolfe, P.S.; Garg, K.; McCool, J.M.; Rodriguez, I.A.; Bowlin, G.L. The use of natural polymers in tissue engineering: A focus on electrospun extracellular matrix analogues. *Polymers* **2010**, *2*, 522–553. [CrossRef]
98. Keshvardoostchokami, M.; Majidi, S.S.; Huo, P.; Ramachandran, R.; Chen, M.; Liu, B. Electrospun nanofibers of natural and synthetic polymers as artificial extracellular matrix for tissue engineering. *Nanomaterials* **2020**, *11*, 21. [CrossRef] [PubMed]
99. Tong, X.; Pan, W.; Su, T.; Zhang, M.; Dong, W.; Qi, X. Recent advances in natural polymer-based drug delivery systems. *React. Funct. Polym.* **2020**, *148*, 104501. [CrossRef]
100. Janoušková, O. Synthetic polymer scaffolds for soft tissue engineering. *Physiol. Res.* **2018**, *67*, S335–S348. [CrossRef]
101. Ghasemi-Mobarakeh, L.; Kolahreez, D.; Ramakrishna, S.; Williams, D. Key terminology in biomaterials and biocompatibility. *Curr. Opin. Biomed. Eng.* **2019**, *10*, 45–50. [CrossRef]
102. Nagam Hanumantharao, S. *A 3D Biomimetic Scaffold Using Electrospinning for Tissue Engineering Applications*; Michigan Technological University: Houghton, MI, USA, 2017; p. 75.
103. Ricotti, L.; Polini, A.; Genchi, G.G.; Ciofani, G.; Iandolo, D.; Vazão, H.; Mattoli, V.; Ferreira, L.; Menciassi, A.; Pisignano, D. Proliferation and skeletal myotube formation capability of C2C12 and H9c2 cells on isotropic and anisotropic electrospun nanofibrous PHB scaffolds. *Biomed. Mater.* **2012**, *7*, 035010. [CrossRef] [PubMed]
104. Fujie, T.; Shi, X.; Ostrovidov, S.; Liang, X.; Nakajima, K.; Chen, Y.; Wu, H.; Khademhosseini, A. Spatial coordination of cell orientation directed by nanoribbon sheets. *Biomaterials* **2015**, *53*, 86–94. [CrossRef] [PubMed]
105. Jana, S.; Leung, M.; Chang, J.; Zhang, M. Effect of nano- and micro-scale topological features on alignment of muscle cells and commitment of myogenic differentiation. *Biofabrication* **2014**, *6*, 035012. [CrossRef]
106. Das, S.; Browne, K.D.; Laimo, F.A.; Maggiore, J.C.; Hilman, M.C.; Kaisaier, H.; Aguilar, C.A.; Ali, Z.S.; Mourkioti, F.; Cullen, D.K. Pre-innervated tissue-engineered muscle promotes a pro-regenerative microenvironment following volumetric muscle loss. *Commun. Biol.* **2020**, *3*, 330. [CrossRef]

107. Ma, P.X.; Zhang, R. Microtubular architecture of biodegradable polymer scaffolds. *J. Biomed. Mater. Res.* **2001**, *56*, 469–477. [CrossRef]
108. Rowland, D.C.; Aquilina, T.; Klein, A.; Hakimi, O.; Alexis-Mouthuy, P.; Carr, A.J.; Snelling, S.J. A comparative evaluation of the effect of polymer chemistry and fiber orientation on mesenchymal stem cell differentiation. *J. Biomed. Mater. Res. A* **2016**, *104*, 2843–2853. [CrossRef] [PubMed]
109. Hu, L.-Y.; Mileti, C.J.; Loomis, T.; Brashear, S.E.; Ahmad, S.; Chellakudam, R.R.; Wohlgemuth, R.P.; Gionet-Gonzales, M.A.; Leach, J.K.; Smith, L.R. Skeletal muscle progenitors are sensitive to collagen architectural features of fibril size and cross linking. *Am. J. Physiol. Cell Physiol.* **2021**, *321*, C330–C342. [CrossRef] [PubMed]
110. Suresh, S.; Becker, A.; Glasmacher, B. Impact of apparatus orientation and gravity in electrospinning—A review of empirical evidence. *Polymers* **2020**, *12*, 2448. [CrossRef]
111. Suresh, S.; Gryshkov, O.; Glasmacher, B. Impact of setup orientation on blend electrospinning of poly-ε-caprolactone-gelatin scaffolds for vascular tissue engineering. *Int. J. Artif. Organs* **2018**, *41*, 801–810. [CrossRef] [PubMed]
112. Nagam Hanumantharao, S.; Rao, S. Multi-functional electrospun nanofibers from polymer blends for scaffold tissue engineering. *Fibers* **2019**, *7*, 66. [CrossRef]
113. Simon, C.G., Jr.; Kumar, G.; Tison, C.K. *Nanofiber Scaffolds Induce Morphological Changes in hBMSCs Critical for Osteogenic Differentiation*; NIST: Gaithersburg, MD, USA, 2011.
114. Kumar, G.; Tison, C.K.; Chatterjee, K.; Pine, P.S.; McDaniel, J.H.; Salit, M.L.; Young, M.F.; Simon, C.G. The determination of stem cell fate by 3D scaffold structures through the control of cell shape. *Biomaterials* **2011**, *32*, 9188–9196. [CrossRef] [PubMed]
115. Farooque, T.M.; Camp, C.H., Jr.; Tison, C.K.; Kumar, G.; Parekh, S.H.; Simon, C.G., Jr. Measuring stem cell dimensionality in tissue scaffolds. *Biomaterials* **2014**, *35*, 2558–2567. [CrossRef]
116. Tutak, W.; Jyotsnendu, G.; Bajcsy, P.; Simon, C.G. Nanofiber scaffolds influence organelle structure and function in bone marrow stromal cells. *J. Biomed. Mater. Res. B Appl. Biomater.* **2017**, *105*, 989–1001. [CrossRef]
117. Thomas, C.H.; Collier, J.H.; Sfeir, C.S.; Healy, K.E. Engineering gene expression and protein synthesis by modulation of nuclear shape. *Proc. Natl. Acad. Sci. USA* **2002**, *99*, 1972–1977. [CrossRef]
118. Tsimbouri, P.M.; Murawski, K.; Hamilton, G.; Herzyk, P.; Oreffo, R.O.; Gadegaard, N.; Dalby, M.J. A genomics approach in determining nanotopographical effects on MSC phenotype. *Biomaterials* **2013**, *34*, 2177–2184. [CrossRef]
119. Chen, D.; Sarkar, S.; Candia, J.; Florczyk, S.J.; Bodhak, S.; Driscoll, M.K.; Simon, C.G.; Dunkers, J.P.; Losert, W. Machine learning based methodology to identify cell shape phenotypes associated with microenvironmental cues. *Biomaterials* **2016**, *104*, 104–118. [CrossRef]
120. Chen, D.; Dunkers, J.P.; Losert, W.; Sarkar, S. Early time-point cell morphology classifiers successfully predict human bone marrow stromal cell differentiation modulated by fiber density in nanofiber scaffolds. *Biomaterials* **2021**, *274*, 120812. [CrossRef]
121. Xie, J.; Shen, H.; Yuan, G.; Lin, K.; Su, J. The effects of alignment and diameter of electrospun fibers on the cellular behaviors and osteogenesis of BMSCs. *Mater. Sci. Eng. C Mater. Biol. Appl.* **2021**, *120*, 111787. [CrossRef] [PubMed]
122. Ma, J.; He, X.; Jabbari, E. Osteogenic differentiation of marrow stromal cells on random and aligned electrospun poly(L-lactide) nanofibers. *Ann. Biomed. Eng.* **2011**, *39*, 14–25. [CrossRef] [PubMed]
123. Pandey, S.; Rathore, K.; Johnson, J.; Cekanova, M. Aligned nanofiber material supports cell growth and increases osteogenesis in canine adipose-derived mesenchymal stem cells in vitro. *J. Biomed. Mater. Res. A* **2018**, *106*, 1780–1788. [CrossRef]
124. Newman, P.; Galenano-Niño, J.L.; Graney, P.; Razal, J.M.; Minett, A.I.; Ribas, J.; Ovalle-Robles, R.; Biro, M.; Zreiqat, H. Relationship between nanotopographical alignment and stem cell fate with live imaging and shape analysis. *Sci. Rep.* **2016**, *6*, 37909. [CrossRef]
125. Kolambkar, Y.M.; Bajin, M.; Wojtowicz, A.; Hutmacher, D.W.; García, A.J.; Guldberg, R.E. Nanofiber orientation and surface functionalization modulate human mesenchymal stem cell behavior in vitro. *Tissue Eng. Part A* **2014**, *20*, 398–409. [CrossRef]
126. Lanfer, B.; Seib, F.P.; Freudenberg, U.; Stamov, D.; Bley, T.; Bornhäuser, M.; Werner, C. The growth and differentiation of mesenchymal stem and progenitor cells cultured on aligned collagen matrices. *Biomaterials* **2009**, *30*, 5950–5958. [CrossRef]
127. Kim, M.-J.; Lee, B.; Yang, K.; Park, J.; Jeon, S.; Um, S.H.; Kim, D.-I.; Im, S.G.; Cho, S.-W. BMP-2 peptide-functionalized nanopatterned substrates for enhanced osteogenic differentiation of human mesenchymal stem cells. *Biomaterials* **2013**, *34*, 7236–7246. [CrossRef]
128. Vo, T.N.; Tabata, Y.; Mikos, A.G. Effects of cellular parameters on the in vitro osteogenic potential of dual-gelling mesenchymal stem cell-laden hydrogels. *J. Biomater. Sci. Polym. Ed.* **2016**, *27*, 1277–1290. [CrossRef] [PubMed]
129. Hu, X.; Park, S.-H.; Gil, E.S.; Xia, X.-X.; Weiss, A.; Kaplan, D.L. The influence of elasticity and surface roughness on myogenic and osteogenic-differentiation of cells on silk-elastin biomaterials. *Biomaterials* **2011**, *32*, 8979–8989. [CrossRef] [PubMed]
130. Shin, Y.C.; Lee, J.H.; Jin, L.; Kim, M.J.; Kim, Y.-J.; Hyun, J.K.; Jung, T.-G.; Hong, S.W.; Han, D.-W. Stimulated myoblast differentiation on graphene oxide-impregnated PLGA-collagen hybrid fibre matrices. *J. Nanobiotechnol.* **2015**, *13*, 21. [CrossRef]
131. Shimizu, K.; Fujita, H.; Nagamori, E. Alignment of skeletal muscle myoblasts and myotubes using linear micropatterned surfaces ground with abrasives. *Biotechnol. Bioeng.* **2009**, *103*, 631–638. [CrossRef] [PubMed]
132. Patel, A.; Mukundan, S.; Wang, W.; Karumuri, A.; Sant, V.; Mukhopadhyay, S.M.; Sant, S. Carbon-based hierarchical scaffolds for myoblast differentiation: Synergy between nano-functionalization and alignment. *Acta Biomater.* **2016**, *32*, 77–88. [CrossRef]
133. Yeo, M.; Kim, G. Nano/microscale topographically designed alginate/PCL scaffolds for inducing myoblast alignment and myogenic differentiation. *Carbohydr. Polym.* **2019**, *223*, 115041. [CrossRef] [PubMed]

134. Zhou, J.; Yang, X.; Liu, W.; Wang, C.; Shen, Y.; Zhang, F.; Zhu, H.; Sun, H.; Chen, J.; Lam, J.; et al. Injectable OPF/graphene oxide hydrogels provide mechanical support and enhance cell electrical signaling after implantation into myocardial infarct. *Theranostics* **2018**, *8*, 3317–3330. [CrossRef] [PubMed]
135. Malikmammadov, E.; Tanir, T.E.; Kiziltay, A.; Hasirci, V.; Hasirci, N. PCL and PCL-based materials in biomedical applications. *J. Biomater. Sci. Polym. Ed.* **2018**, *29*, 863–893. [CrossRef]
136. Homaeigohar, S.; Boccaccini, A.R. Nature-Derived and Synthetic Additives to poly(ε-Caprolactone) Nanofibrous Systems for Biomedicine; an Updated Overview. *Front. Chem.* **2022**, *9*, 809676. [CrossRef] [PubMed]
137. Gao, J.; Chen, S.; Tang, D.; Jiang, L.; Shi, J.; Wang, S. Mechanical Properties and Degradability of Electrospun PCL/PLGA Blended Scaffolds as Vascular Grafts. *Trans. Tianjin Univ.* **2018**, *25*, 152–160. [CrossRef]
138. Leung, M.; Cooper, A.; Jana, S.; Tsao, C.-T.; Petrie, T.A.; Zhang, M. Nanofiber-based in vitro system for high myogenic differentiation of human embryonic stem cells. *Biomacromolecules* **2013**, *14*, 4207–4216. [CrossRef]
139. Jana, S.; Cooper, A.; Zhang, M. Chitosan scaffolds with unidirectional microtubular pores for large skeletal myotube generation. *Adv. Healthc. Mater.* **2013**, *2*, 557–561. [CrossRef]
140. Stern, M.M.; Myers, R.L.; Hammam, N.; Stern, K.A.; Eberli, D.; Kritchevsky, S.B.; Soker, S.; Van Dyke, M. The influence of extracellular matrix derived from skeletal muscle tissue on the proliferation and differentiation of myogenic progenitor cells ex vivo. *Biomaterials* **2009**, *30*, 2393–2399. [CrossRef] [PubMed]
141. Wingate, K.; Bonani, W.; Tan, Y.; Bryant, S.; Tan, W. Compressive elasticity of three-dimensional nanofiber matrix directs mesenchymal stem cell differentiation to vascular cells with endothelial or smooth muscle cell markers. *Acta Biomater.* **2012**, *8*, 1440–1449. [CrossRef] [PubMed]
142. Somaiah, C.; Kumar, A.; Mawrie, D.; Sharma, A.; Patil, S.D.; Bhattacharyya, J.; Swaminathan, R.; Jaganathan, B.G. Collagen Promotes Higher Adhesion, Survival and Proliferation of Mesenchymal Stem Cells. *PLoS ONE* **2015**, *10*, e0145068. [CrossRef] [PubMed]
143. Bertram, U.; Steiner, D.; Poppitz, B.; Dippold, D.; Köhn, K.; Beier, J.P.; Detsch, R.; Boccaccini, A.R.; Schubert, D.W.; Horch, R.E.; et al. Vascular Tissue Engineering: Effects of Integrating Collagen into a PCL Based Nanofiber Material. *BioMed Res. Int.* **2017**, *2017*, 9616939. [CrossRef]
144. Choi, J.S.; Lee, S.J.; Christ, G.J.; Atala, A.; Yoo, J.J. The influence of electrospun aligned poly(epsilon-caprolactone)/collagen nanofiber meshes on the formation of self-aligned skeletal muscle myotubes. *Biomaterials* **2008**, *29*, 2899–2906. [CrossRef]
145. Brzeska, J.; Tercjak, A.; Sikorska, W.; Kowalczuk, M.; Rutkowska, M. Morphology and Physicochemical Properties of Branched Polyurethane/Biopolymer Blends. *Polymers* **2019**, *12*, 16. [CrossRef]
146. McClure, M.J.; Garg, K.; Simpson, D.G.; Ryan, J.J.; Sell, S.A.; Bowlin, G.L.; Ericksen, J.J. The influence of platelet-rich plasma on myogenic differentiation. *J. Tissue Eng. Regen. Med.* **2016**, *10*, E239–E249. [CrossRef]
147. Shin, Y.C.; Kim, C.; Song, S.-J.; Jun, S.; Kim, C.-S.; Hong, S.W.; Hyon, S.-H.; Han, D.-W.; Oh, J.-W. Ternary Aligned Nanofibers of RGD Peptide-Displaying M13 Bacteriophage/PLGA/Graphene Oxide for Facilitated Myogenesis. *Nanotheranostics* **2018**, *2*, 144–156. [CrossRef]
148. Wen, F.; Wong, H.K.; Tay, C.Y.; Yu, H.; Li, H.; Yu, T.; Tijore, A.; Boey, F.Y.C.; Venkatraman, S.S.; Tan, L.P.; et al. Induction of myogenic differentiation of human mesenchymal stem cells cultured on Notch agonist (Jagged-1) modified biodegradable scaffold surface. *ACS Appl. Mater. Interfaces* **2014**, *6*, 1652–1661. [CrossRef] [PubMed]
149. Jahanmard, F.; Eslaminejad, M.B.; Amani-Tehran, M.; Zarei, F.; Rezaei, N.; Croes, M.; Yavari, S.A. Incorporation of F-MWCNTs into electrospun nanofibers regulates osteogenesis through stiffness and nanotopography. *Mater. Sci. Eng. C Mater. Biol. Appl.* **2020**, *106*, 110163. [CrossRef]
150. Gaharwar, A.K.; Mukundan, S.; Karaca, E.; Dolatshahi-Pirouz, A.; Patel, A.; Rangarajan, K.; Mihaila, S.M.; Iviglia, G.; Zhang, H.; Khademhosseini, A. Nanoclay-enriched poly(varepsilon-caprolactone) electrospun scaffolds for osteogenic differentiation of human mesenchymal stem cells. *Tissue Eng. Part A* **2014**, *20*, 2088–2101. [CrossRef]
151. Wang, X.; Gittens, R.A.; Song, R.; Tannenbaum, R.; Olivares-Navarrete, R.; Schwartz, Z.; Chen, H.; Boyan, B.D. Effects of structural properties of electrospun TiO2 nanofiber meshes on their osteogenic potential. *Acta Biomater.* **2012**, *8*, 878–885. [CrossRef]
152. Chen, H.; Huang, X.; Zhang, M.; Damanik, F.; Baker, M.B.; Leferink, A.; Yuan, H.; Truckenmüller, R.; van Blitterswijk, C.; Moroni, L. Tailoring surface nanoroughness of electrospun scaffolds for skeletal tissue engineering. *Acta Biomater.* **2017**, *59*, 82–93. [CrossRef]
153. Faia-Torres, A.B.; Charnley, M.; Goren, T.; Guimond-Lischer, S.; Rottmar, M.; Maniura-Weber, K.; Spencer, N.D.; Reis, R.L.; Textor, M.; Neves, N.M. Osteogenic differentiation of human mesenchymal stem cells in the absence of osteogenic supplements: A surface-roughness gradient study. *Acta Biomater.* **2015**, *28*, 64–75. [CrossRef]
154. Gittens, R.A.; McLachlan, T.; Olivares-Navarrete, R.; Cai, Y.; Berner, S.; Tannenbaum, R.; Schwartz, Z.; Sandhage, K.H.; Boyan, B.D. The effects of combined micron-/submicron-scale surface roughness and nanoscale features on cell proliferation and differentiation. *Biomaterials* **2011**, *32*, 3395–3403. [CrossRef]
155. McBeath, R.; Pirone, D.M.; Nelson, C.M.; Bhadriraju, K.; Chen, C.S. Cell shape, cytoskeletal tension, and RhoA regulate stem cell lineage commitment. *Dev. Cell* **2004**, *6*, 483–495. [CrossRef] [PubMed]
156. Sarkar, S. Roles of Nanofiber Scaffold Structure and Chemistry in Directing Human Bone Marrow Stromal Cell Response. *Adv. Tissue Eng. Regen. Med.* **2016**, *1*, 6–18. [CrossRef]
157. Nair, L.S.; Laurencin, C.T. Biodegradable polymers as biomaterials. *Prog. Polym. Sci.* **2007**, *32*, 762–798. [CrossRef]

158. Moradi, Y.; Atyabi, S.A.; Ghiassadin, A.; Bakhshi, H.; Irani, S.; Dadgar, N. Cold Atmosphere Plasma Modification on Beta-Carotene-Loaded Nanofibers to Enhance Osteogenic Differentiation. *Fibers Polym.* **2021**, *23*, 18–27. [CrossRef]
159. Atyabi, S.M.; Sharifi, F.; Irani, S.; Zandi, M.; Mivehchi, H.; Nagheh, Z. Cell Attachment and Viability Study of PCL Nano-fiber Modified by Cold Atmospheric Plasma. *Cell Biochem. Biophys.* **2016**, *74*, 181–190. [CrossRef]
160. Kooshki, H.; Ghollasi, M.; Halabian, R.; Kazemi, N.M. Osteogenic differentiation of preconditioned bone marrow mesenchymal stem cells with lipopolysaccharide on modified poly-l-lactic-acid nanofibers. *J. Cell. Physiol.* **2019**, *234*, 5343–5353. [CrossRef] [PubMed]
161. Xing, Y.; Zhang, Y.; Jia, L.; Xu, X. Lipopolysaccharide from Escherichia coli stimulates osteogenic differentiation of human periodontal ligament stem cells through Wnt/beta-catenin-induced TAZ elevation. *Mol. Oral Microbiol.* **2019**, *34*, omi.12249.
162. Onak, G.; Şen, M.; Horzum, N.; Ercan, U.K.; Yaralı, Z.B.; Garipcan, B.; Karaman, O. Aspartic and Glutamic Acid Templated Peptides Conjugation on Plasma Modified Nanofibers for Osteogenic Differentiation of Human Mesenchymal Stem Cells: A Comparative Study. *Sci. Rep.* **2018**, *8*, 17620. [CrossRef]
163. Liu, H.; Li, W.; Wen, W.; Luo, B.; Liu, M.; Ding, S.; Zhou, C. Mechanical properties and osteogenic activity of poly(l-lactide) fibrous membrane synergistically enhanced by chitosan nanofibers and polydopamine layer. *Mater. Sci. Eng. C Mater. Biol. Appl.* **2017**, *81*, 280–290. [CrossRef] [PubMed]
164. Sanaei-Rad, P.; Kashi, T.-S.J.; Seyedjafari, E.; Soleimani, M. Enhancement of stem cell differentiation to osteogenic lineage on hydroxyapatite-coated hybrid PLGA/gelatin nanofiber scaffolds. *Biologicals* **2016**, *44*, 511–516. [CrossRef]
165. Parvathi, K.; Krishnan, A.G.; Anitha, A.; Jayakumar, R.; Nair, M.B. Poly(L-lactic acid) nanofibers containing *Cissus quadrangularis* induced osteogenic differentiation in vitro. *Int. J. Biol. Macromol.* **2018**, *110*, 514–521. [CrossRef]
166. Zhang, K.; Wang, Y.; Sun, T.; Wang, B.; Zhang, H. Bioinspired Surface Functionalization for Improving Osteogenesis of Electrospun Polycaprolactone Nanofibers. *Langmuir* **2018**, *34*, 15544–15550. [CrossRef]
167. Seyedjafari, E.; Soleimani, M.; Ghaemi, N.; Shabani, I. Nanohydroxyapatite-coated electrospun poly(l-lactide) nanofibers enhance osteogenic differentiation of stem cells and induce ectopic bone formation. *Biomacromolecules* **2010**, *11*, 3118–3125. [CrossRef] [PubMed]
168. Engler, A.J.; Sen, S.; Sweeney, H.L.; Discher, D.E. Matrix elasticity directs stem cell lineage specification. *Cell* **2006**, *126*, 677–689. [CrossRef] [PubMed]
169. *ASTM F3369-19e1*; Standard Guide for Assessing the Skeletal Myoblast Phenotype. ASTM International: West Conshoshocken, PA, USA, 2019.
170. Engler, A.J.; Griffin, M.A.; Sen, S.; Bönnemann, C.G.; Sweeney, H.L.; Discher, D.E. Myotubes differentiate optimally on substrates with tissue-like stiffness: Pathological implications for soft or stiff microenvironments. *J. Cell Biol.* **2004**, *166*, 877–887. [CrossRef]
171. Xu, J.; Xie, Y.; Zhang, H.; Ye, Z.; Zhang, W. Fabrication of PLGA/MWNTs composite electrospun fibrous scaffolds for improved myogenic differentiation of C2C12 cells. *Colloids Surf. B Biointerfaces* **2014**, *123*, 907–915. [CrossRef] [PubMed]
172. Uribe-Gomez, J.; Posada-Murcia, A.; Shukla, A.; Alkhamis, H.; Salehi, S.; Ionov, L. Soft Elastic Fibrous Scaffolds for Muscle Tissue Engineering by Touch Spinning. *ACS Appl. Bio Mater.* **2021**, *4*, 5585–5597. [CrossRef] [PubMed]
173. Nam, J.; Johnson, J.; Lannutti, J.J.; Agarwal, S. Modulation of embryonic mesenchymal progenitor cell differentiation via control over pure mechanical modulus in electrospun nanofibers. *Acta Biomater.* **2011**, *7*, 1516–1524. [CrossRef] [PubMed]
174. Fu, C.; Bai, H.; Zhu, J.; Niu, Z.; Wang, Y.; Li, J.; Yang, X.; Bai, Y. Enhanced cell proliferation and osteogenic differentiation in electrospun PLGA/hydroxyapatite nanofibre scaffolds incorporated with graphene oxide. *PLoS ONE* **2017**, *12*, e0188352. [CrossRef] [PubMed]
175. Rho, J.Y.; Ashman, R.B.; Turner, C.H. Young's modulus of trabecular and cortical bone material: Ultrasonic and microtensile measurements. *J. Biomech.* **1993**, *26*, 111–119. [CrossRef]
176. Wang, Z.; Liang, R.; Jiang, X.; Xie, J.; Cai, P.; Chen, H.; Zhan, X.; Lei, D.; Zhao, J.; Zheng, L. Electrospun PLGA/PCL/OCP nanofiber membranes promote osteogenic differentiation of mesenchymal stem cells (MSCs). *Mater. Sci. Eng. C Mater. Biol. Appl.* **2019**, *104*, 109796. [CrossRef]
177. Daňková, J.; Buzgo, M.; Vejpravová, J.; Kubíčková, S.; Sovková, V.; Vysloužilová, L.; Mantlíková, A.; Nečas, A.; Amler, E. Highly efficient mesenchymal stem cell proliferation on poly-epsilon-caprolactone nanofibers with embedded magnetic nanoparticles. *Int. J. Nanomed.* **2015**, *10*, 7307–7317. [CrossRef]
178. Bateni, F.; Motlagh, G.H. Electrospun polyamide/graphene oxide nanofibers as fillers for polyethylene: Preparation and characterization. *J. Appl. Polym. Sci.* **2021**, *139*, 51506. [CrossRef]
179. Ramazani, S.; Karimi, M. Aligned poly(epsilon-caprolactone)/graphene oxide and reduced graphene oxide nanocomposite nanofibers: Morphological, mechanical and structural properties. *Mater. Sci. Eng. C Mater. Biol. Appl.* **2015**, *56*, 325–334. [CrossRef]
180. Yao, Q.; Fuglsby, K.E.; Zheng, X.; Sun, H. Nanoclay-functionalized 3D nanofibrous scaffolds promote bone regeneration. *J. Mater. Chem. B* **2020**, *8*, 3842–3851. [CrossRef]
181. Yi, Q.; Wen, X.; Li, L.; He, B.; Wu, Y.; Nie, Y.; Gu, Z. The polymeric crystallinity effect on the responses of bone marrow stromal cells. *e-Polymers* **2009**, *9*, 42. [CrossRef]
182. Cui, H.; Sinko, P.J. The role of crystallinity on differential attachment/proliferation of osteoblasts and fibroblasts on poly (caprolactone-co-glycolide) polymeric surfaces. *Front. Mater. Sci.* **2011**, *6*, 47–59. [CrossRef]

183. Müller, W.E.; Ackermann, M.; Al-Nawas, B.; Righesso, L.A.; Muñoz-Espí, R.; Tolba, E.; Neufurth, M.; Schröder, H.C.; Wang, X. Amplified morphogenetic and bone forming activity of amorphous versus crystalline calcium phosphate/polyphosphate. *Acta Biomater.* **2020**, *118*, 233–247. [CrossRef] [PubMed]
184. Seetharam, A.; Abad, J.; Baessler, A.; Badman, B.L. Use of a Nanofiber Resorbable Scaffold During Rotator Cuff Repair: Surgical Technique and Results After Repair of Small- to Medium-Sized Tears. *Orthop. J. Sport. Med.* **2022**, *10*, 23259671221094848. [CrossRef] [PubMed]
185. Chaudhari, A.A.; Vig, K.; Baganizi, D.R.; Sahu, R.; Dixit, S.; Dennis, V.; Singh, S.R.; Pillai, S.R. Future Prospects for Scaffolding Methods and Biomaterials in Skin Tissue Engineering: A Review. *Int. J. Mol. Sci.* **2016**, *17*, 1974. [CrossRef]
186. Phillips, H. RenovoDerm Receives FDA Clearance for Proprietary Product, in Newswire. 2018. Available online: https://www.newswire.com/news/renovoderm-receives-fda-clearance-for-proprietary-product-20370988 (accessed on 3 March 2022).
187. U.S. Food and Drug Administration. *510(k) Premarket Notification—Phoenix Wound Matrix*; U.S. Food and Drug Administration: Silver Spring, MD, USA, 2018.
188. Schulz, A.; Fuchs, P.; Heitzmann, W.; Kanho, C.; Schiefer, J. Our Initial Experience In The Customized Treatment Of Donor Site And Burn Wounds With A New Nanofibrous Temporary Epidermal Layer. *Ann. Burn. Fire Disasters* **2021**, *34*, 58–66.
189. Sadeghianmaryan, A.; Karimi, Y.; Naghieh, S.; Sardroud, H.A.; Gorji, M.; Chen, X. Electrospinning of Scaffolds from the Polycaprolactone/Polyurethane Composite with Graphene Oxide for Skin Tissue Engineering. *Appl. Biochem. Biotechnol.* **2020**, *191*, 567–578. [CrossRef]
190. Keirouz, A.; Zakharova, M.; Kwon, J.; Robert, C.; Koutsos, V.; Callanan, A.; Chen, X.; Fortunato, G.; Radacsi, N. High-throughput production of silk fibroin-based electrospun fibers as biomaterial for skin tissue engineering applications. *Mater. Sci. Eng. C* **2020**, *112*, 110939. [CrossRef]
191. Movahedi, M.; Asefnejad, A.; Rafienia, M.; Khorasani, M.T. Potential of novel electrospun core-shell structured polyurethane/starch (hyaluronic acid) nanofibers for skin tissue engineering: In vitro and in vivo evaluation. *Int. J. Biol. Macromol.* **2020**, *146*, 627–637. [CrossRef]
192. Narayanan, K.B.; Park, G.T.; Han, S.S. Electrospun poly(vinyl alcohol)/reduced graphene oxide nanofibrous scaffolds for skin tissue engineering. *Colloids Surf. B Biointerfaces* **2020**, *191*, 110994. [CrossRef] [PubMed]
193. Rathinavel, S.; Ekambaram, S.; Korrapati, P.S.; Sangeetha, D. Design and fabrication of electrospun SBA-15-incorporated PVA with curcumin: A biomimetic nanoscaffold for skin tissue engineering. *Biomed. Mater.* **2020**, *15*, 035009. [CrossRef] [PubMed]
194. Lopresti, F.; Campora, S.; Tirri, G.; Capuana, E.; Pavia, F.C.; Brucato, V.; Ghersi, G.; La Carrubba, V. Core-shell PLA/Kef hybrid scaffolds for skin tissue engineering applications prepared by direct kefiran coating on PLA electrospun fibers optimized via air-plasma treatment. *Mater. Sci. Eng. C* **2021**, *127*, 112248. [CrossRef] [PubMed]
195. Ruggeri, M.; Bianchi, E.; Rossi, S.; Boselli, C.; Cornaglia, A.I.; Malavasi, L.; Carzino, R.; Suarato, G.; Sánchez-Espejo, R.; Athanassiou, A.; et al. Maltodextrin-amino acids electrospun scaffolds cross-linked with Maillard-type reaction for skin tissue engineering. *Mater. Sci. Eng. C* **2021**, *133*, 112593. [CrossRef]
196. Zarei, M.; Samimi, A.; Khorram, M.; Abdi, M.M.; Golestaneh, S.I. Fabrication and characterization of conductive polypyrrole/chitosan/collagen electrospun nanofiber scaffold for tissue engineering application. *Int. J. Biol. Macromol.* **2021**, *168*, 175–186. [CrossRef]
197. Ababzadeh, S.; Farzin, A.; Goodarzi, A.; Karimi, R.; Farahani, M.S.; Farsani, M.E.; Gharibzad, K.; Zahiri, M.; Ai, J. High porous electrospun poly (ε-caprolactone)/gelatin/MgO scaffolds preseeded with endometrial stem cells promote tissue regeneration in full-thickness skin wounds: An in vivo study. *J. Biomed. Mater. Res. Part B Appl. Biomater.* **2020**, *108*, 2961–2970. [CrossRef] [PubMed]
198. Fathi, A.; Khanmohammadi, M.; Goodarzi, A.; Foroutani, L.; Mobarakeh, Z.T.; Saremi, J.; Arabpour, Z.; Ai, J. Fabrication of chitosan-polyvinyl alcohol and silk electrospun fiber seeded with differentiated keratinocyte for skin tissue regeneration in animal wound model. *J. Biol. Eng.* **2020**, *14*, 27. [CrossRef]
199. Ghorbani, M.; Nezhad-Mokhtari, P.; Sohrabi, H.; Roshangar, L. Electrospun chitosan/nanocrystalline cellulose-graft-poly(N-vinylcaprolactam) nanofibers as the reinforced scaffold for tissue engineering. *J. Mater. Sci.* **2020**, *55*, 2176–2185. [CrossRef]
200. Chen, J.; Zhang, G.; Zhao, Y.; Zhou, M.; Zhong, A.; Sun, J. Promotion of skin regeneration through co-axial electrospun fibers loaded with basic fibroblast growth factor. *Adv. Compos. Hybrid Mater.* **2022**, *5*, 1111–1125. [CrossRef]
201. Goudarzi, Z.M.; Behzad, T.; Ghasemi-Mobarakeh, L.; Kharaziha, M. An investigation into influence of acetylated cellulose nanofibers on properties of PCL/Gelatin electrospun nanofibrous scaffold for soft tissue engineering. *Polymer* **2021**, *213*, 123313. [CrossRef]
202. Ramos-Rodriguez, D.H.; MacNeil, S.; Claeyssens, F.; Ortega Asencio, I. Fabrication of Topographically Controlled Electrospun Scaffolds to Mimic the Stem Cell Microenvironment in the Dermal-Epidermal Junction. *ACS Biomater. Sci. Eng.* **2021**, *7*, 2803–2813. [CrossRef] [PubMed]
203. Ji, X.; Li, R.; Liu, G.; Jia, W.; Sun, M.; Liu, Y.; Luo, Y.; Cheng, Z. Phase separation-based electrospun Janus nanofibers loaded with Rana chensinensis skin peptides/silver nanoparticles for wound healing. *Mater. Des.* **2021**, *207*, 109864. [CrossRef]
204. Ji, X.; Li, R.; Jia, W.; Liu, G.; Luo, Y.-G.; Cheng, Z. Co-Axial Fibers with Janus-Structured Sheaths by Electrospinning Release Corn Peptides for Wound Healing. *ACS Appl. Bio Mater.* **2020**, *3*, 6430–6438. [CrossRef] [PubMed]

205. Chandika, P.; Oh, G.-W.; Heo, S.-Y.; Kim, S.-C.; Kim, T.-H.; Kim, M.-S.; Jung, W.-K. Electrospun porous bilayer nano-fibrous fish collagen/PCL bio-composite scaffolds with covalently cross-linked chitooligosaccharides for full-thickness wound-healing applications. *Mater. Sci. Eng. C* **2021**, *121*, 111871. [CrossRef]
206. Li, P.; Ruan, L.; Wang, R.; Liu, T.; Song, G.; Gao, X.; Jiang, G.; Liu, X. Electrospun Scaffold of Collagen and Polycaprolactone Containing ZnO Quantum Dots for Skin Wound Regeneration. *J. Bionic Eng.* **2021**, *18*, 1378–1390. [CrossRef]
207. Madub, K.; Goonoo, N.; Gimié, F.; Arsa, I.A.; Schönherr, H.; Bhaw-Luximon, A. Green seaweeds ulvan-cellulose scaffolds enhance in vitro cell growth and in vivo angiogenesis for skin tissue engineering. *Carbohydr. Polym.* **2021**, *251*, 117025. [CrossRef]
208. Atila, D.; Hasirci, V.; Tezcaner, A. Coaxial electrospinning of composite mats comprised of core/shell poly(methyl methacrylate)/silk fibroin fibers for tissue engineering applications. *J. Mech. Behav. Biomed. Mater.* **2022**, *128*, 105105. [CrossRef] [PubMed]
209. Tourlomousis, F.; Jia, C.; Karydis, T.; Mershin, A.; Wang, H.; Kalyon, D.M.; Chang, R.C. Machine learning metrology of cell confinement in melt electrowritten three-dimensional biomaterial substrates. *Microsyst. Nanoeng.* **2019**, *5*, 15. [CrossRef]
210. Niu, Y.; Galluzzi, M.; Fu, M.; Hu, J.; Xia, H. In vivo performance of electrospun tubular hyaluronic acid/collagen nanofibrous scaffolds for vascular reconstruction in the rabbit model. *J. Nanobiotechnol.* **2021**, *19*, 349. [CrossRef]
211. Kandzari, D.E.; Birkemeyer, R. PK Papyrus covered stent: Device description and early experience for the treatment of coronary artery perforations. *Catheter. Cardiovasc. Interv.* **2019**, *94*, 564–568. [CrossRef]
212. Hernández-Enríquez, M.; Belle, L.; Madiot, H.; Pansieri, M.; Souteyrand, G.; de Poli, F.; Piot, C.; Boueri, Z.; Gerbaud, E.; Boiffard, E.; et al. Use and outcomes of the PK Papyrus covered stent in France: SOS PK Papyrus Registry. *Catheter. Cardiovasc. Interv.* **2021**, *98*, 874–881. [CrossRef]
213. Wu, Y.-L.; Szafron, J.M.; Blum, K.M.; Zbinden, J.C.; Khosravi, M.R.; Best, C.A.; Reinhardt, J.W.; Zheng, Q.; Yi, T.; Shinoka, T.; et al. Electrospun Tissue-Engineered Arterial Graft Thickness Affects Long-Term Composition and Mechanics. *Tissue Eng. Part A* **2020**, *27*, 593–603. [CrossRef] [PubMed]
214. Daum, R.; Visser, D.; Wild, C.; Kutuzova, L.; Schneider, M.; Lorenz, G.; Weiss, M.; Hinderer, S.; Stock, U.A.; Seifert, M.; et al. Fibronectin Adsorption on Electrospun Synthetic Vascular Grafts Attracts Endothelial Progenitor Cells and Promotes Endothelialization in Dynamic In Vitro Culture. *Cells* **2020**, *9*, 778. [CrossRef] [PubMed]
215. Reid, J.A.; Callanan, A. Hybrid cardiovascular sourced extracellular matrix scaffolds as possible platforms for vascular tissue engineering. *J. Biomed. Mater. Res. Part B Appl. Biomater.* **2020**, *108*, 910–924. [CrossRef]
216. Chen, D.; Zhang, L.; Zhang, W.; Tang, Z.; Fu, W.; Hu, R.; Feng, B.; Hong, H.; Zhang, H. Shapeable large-pore electrospun polycaprolactam cotton facilitates the rapid formation of a functional tissue engineered vascular graft. *Mater. Des.* **2020**, *191*, 108631. [CrossRef]
217. Jin, Q.; Fu, Y.; Zhang, G.; Xu, L.; Jin, G.; Tang, L.; Ju, J.; Zhao, W.; Hou, R. Nanofiber electrospinning combined with rotary bioprinting for fabricating small-diameter vessels with endothelium and smooth muscle. *Compos. Part B Eng.* **2022**, *234*, 109691. [CrossRef]
218. Chew, C.H.; Sheu, B.-L.; Chen, A.; Huang, W.-T.; Cheng, T.-M.; Shih, C.-M.; Chang, A.; Chen, C.-C. Tissue-Engineered Vascular Graft with Co-Culture of Smooth Muscle Cells and Human Endothelial Vein Cells on an Electrospun Poly(lactic-co-glycolic acid) Microtube Array Membrane. *Membranes* **2021**, *11*, 732. [CrossRef]
219. Zhao, L.; Li, X.; Yang, L.; Sun, L.; Mu, S.; Zong, H.; Li, Q.; Wang, F.; Song, S.; Yang, C.; et al. Evaluation of remodeling and regeneration of electrospun PCL/fibrin vascular grafts in vivo. *Mater. Sci. Eng. C* **2021**, *118*, 111441. [CrossRef]
220. Kong, X.; He, Y.; Zhou, H.; Gao, P.; Xu, L.; Han, Z.; Le Yang, L.; Wang, M. Chondroitin Sulfate/Polycaprolactone/Gelatin Electrospun Nanofibers with Antithrombogenicity and Enhanced Endothelial Cell Affinity as a Potential Scaffold for Blood Vessel Tissue Engineering. *Nanoscale Res. Lett.* **2021**, *16*, 62. [CrossRef]
221. Tondnevis, F.; Keshvari, H.; Mohandesi, J.A. Fabrication, characterization, and in vitro evaluation of electrospun polyurethane-gelatin-carbon nanotube scaffolds for cardiovascular tissue engineering applications. *J. Biomed. Mater. Res. Part B Appl. Biomater.* **2020**, *108*, 2276–2293. [CrossRef]
222. A Emechebe, G.; O Obiweluozor, F.; Jeong, I.S.; Park, J.-K.; Park, C.H.; Kim, C.S. Merging 3D printing with electrospun biodegradable small-caliber vascular grafts immobilized with VEGF. *Nanomed. Nanotechnol. Biol. Med.* **2020**, *30*, 102306. [CrossRef] [PubMed]
223. Zhou, Y.; Sooriyaarachchi, D.; Tan, G.Z. Fabrication of Nanopores Polylactic Acid Microtubes by Core-Sheath Electrospinning for Capillary Vascularization. *Biomimetics* **2021**, *6*, 15. [CrossRef] [PubMed]
224. Jang, S.R.; Kim, J.I.; Park, C.H.; Kim, C.S. Development of Y-shaped small diameter artificial blood vessel with controlled topography via a modified electrospinning method. *Mater. Lett.* **2020**, *264*, 127113. [CrossRef]
225. Rubenstein, D.A.; Greene, V.K.; Yin, W. Electrospun scaffold fiber orientation regulates endothelial cell and platelet properties associated with angiogenesis and hemocompatibility. *Materialia* **2020**, *14*, 100942. [CrossRef]
226. Liu, F.; Liao, X.; Liu, C.; Li, M.; Chen, Y.; Shao, W.; Weng, K.; Li, F.; Ou, K.; He, J. Poly(l-lactide-co-caprolactone)/tussah silk fibroin nanofiber vascular scaffolds with small diameter fabricated by core-spun electrospinning technology. *J. Mater. Sci.* **2020**, *55*, 7106–7119. [CrossRef]
227. Dou, J.; Wang, Y.; Jin, X.; Li, P.; Wang, L.; Yuan, J.; Shen, J. PCL/sulfonated keratin mats for vascular tissue engineering scaffold with potential of catalytic nitric oxide generation. *Mater. Sci. Eng. C* **2020**, *107*, 110246. [CrossRef]

228. Grasl, C.; Stoiber, M.; Röhrich, M.; Moscato, F.; Bergmeister, H.; Schima, H. Electrospinning of small diameter vascular grafts with preferential fiber directions and comparison of their mechanical behavior with native rat aortas. *Mater. Sci. Eng. C* **2021**, *124*, 112085. [CrossRef]
229. Columbus, S.; Painuly, D.; Nair, R.P.; Krishnan, V.K. Role of PEGylated CdSe-ZnS quantum dots on structural and functional properties of electrospun polycaprolactone scaffolds for blood vessel tissue engineering. *Eur. Polym. J.* **2021**, *151*, 110430. [CrossRef]
230. Rahmati Nejad, M.; Yousefzadeh, M.; and Solouk, A. Electrospun PET/PCL small diameter nanofibrous conduit for biomedical application. *Mater. Sci. Eng. C* **2020**, *110*, 110692. [CrossRef]
231. Gupta, P.; Lorentz, K.L.; Haskett, D.G.; Cunnane, E.M.; Ramaswamy, A.K.; Weinbaum, J.S.; Vorp, D.A.; Mandal, B.B. Bioresorbable silk grafts for small diameter vascular tissue engineering applications: In vitro and in vivo functional analysis. *Acta Biomater.* **2020**, *105*, 146–158. [CrossRef]
232. Matsuzaki, Y.; Iwaki, R.; Reinhardt, J.W.; Chang, Y.-C.; Miyamoto, S.; Kelly, J.; Zbinden, J.; Blum, K.; Mirhaidari, G.; Ulziibayar, A.; et al. The effect of pore diameter on neo-tissue formation in electrospun biodegradable tissue-engineered arterial grafts in a large animal model. *Acta Biomater.* **2020**, *115*, 176–184. [CrossRef]
233. Vermue, I.M.; Begum, R.; Castilho, M.; Rookmaaker, M.B.; Masereeuw, R.; Bouten, C.V.C.; Verhaar, M.C.; Cheng, C. Renal Biology Driven Macro- and Microscale Design Strategies for Creating an Artificial Proximal Tubule Using Fiber-Based Technologies. *ACS Biomater. Sci. Eng.* **2021**, *7*, 4679–4693. [CrossRef]
234. Baskapan, B.; Callanan, A. Electrospinning Fabrication Methods to Incorporate Laminin in Polycaprolactone for Kidney Tissue Engineering. *Tissue Eng. Regen. Med.* **2022**, *19*, 73–82. [CrossRef] [PubMed]
235. Jansen, K.; Castilho, M.; Aarts, S.; Kaminski, M.M.; Lienkamp, S.S.; Pichler, R.; Malda, J.; Vermonden, T.; Jansen, J.; Masereeuw, R. Fabrication of Kidney Proximal Tubule Grafts Using Biofunctionalized Electrospun Polymer Scaffolds. *Macromol. Biosci.* **2019**, *19*, 1800412. [CrossRef]
236. Agueda, J.R.S.; Madrid, J.; Mondragon, J.M.; Lim, J.; Tan, A.; Wang, I.; Duguran, N.; Bondoc, A. Synthesis and Characterization of Electrospun Polyvinylidene Fluoride-based (PVDF) Scaffolds for Renal Bioengineering. *J. Phys. Conf. Ser.* **2021**, *2071*, 012005. [CrossRef]
237. Behtaj, S.; John, J.A.S.; Ekberg, J.A.K.; Rybachuk, M. Neuron-fibrous scaffold interfaces in the peripheral nervous system: A perspective on the structural requirements. *Neural Regen. Res.* **2022**, *17*, 1893–1897. [CrossRef]
238. Castro, V.O.; Merlini, C. Aligned electrospun nerve conduits with electrical activity as a strategy for peripheral nerve regeneration. *Artif. Organs* **2021**, *45*, 813–818. [CrossRef] [PubMed]
239. Behtaj, S.; Ekberg, J.A.K.; John, J.A.S. Advances in Electrospun Nerve Guidance Conduits for Engineering Neural Regeneration. *Pharmaceutics* **2022**, *14*, 219. [CrossRef] [PubMed]
240. Zha, F.; Chen, W.; Lv, G.; Wu, C.; Hao, L.; Meng, L.; Zhang, L.; Yu, D. Effects of surface condition of conductive electrospun nanofiber mats on cell behavior for nerve tissue engineering. *Mater. Sci. Eng. C* **2021**, *120*, 111795. [CrossRef]
241. Chen, T.; Jiang, H.; Li, X.; Zhang, D.; Zhu, Y.; Chen, X.; Yang, H.; Shen, F.; Xia, H.; Zheng, J.; et al. Proliferation and differentiation study of melatonin functionalized polycaprolactone/gelatin electrospun fibrous scaffolds for nerve tissue engineering. *Int. J. Biol. Macromol.* **2022**, *197*, 103–110. [CrossRef]
242. Shen, J.; Wang, J.; Liu, X.; Sun, Y.; Yin, A.; Chai, Y.; Zhang, K.; Wang, C.; Zheng, X. In Situ Prevascularization Strategy with Three-Dimensional Porous Conduits for Neural Tissue Engineering. *ACS Appl. Mater. Interfaces* **2021**, *13*, 50785–50801. [CrossRef] [PubMed]
243. Wang, J.; Xiong, H.; Zhu, T.; Liu, Y.; Pan, H.; Fan, C.; Zhao, X.; Lu, W.W. Bioinspired Multichannel Nerve Guidance Conduit Based on Shape Memory Nanofibers for Potential Application in Peripheral Nerve Repair. *ACS Nano* **2020**, *14*, 12579–12595. [CrossRef] [PubMed]
244. Kong, Y.; Xu, J.; Han, Q.; Zheng, T.; Wu, L.; Li, G.; Yang, Y. Electrospinning porcine decellularized nerve matrix scaffold for peripheral nerve regeneration. *Int. J. Biol. Macromol.* **2022**, *209*, 1867–1881. [CrossRef] [PubMed]
245. Entekhabi, E.; Nazarpak, M.H.; Shafieian, M.; Mohammadi, H.; Firouzi, M.; Hassannejad, Z. Fabrication and in vitro evaluation of 3D composite scaffold based on collagen/hyaluronic acid sponge and electrospun polycaprolactone nanofibers for peripheral nerve regeneration. *J. Biomed. Mater. Res. Part A* **2021**, *109*, 300–312. [CrossRef] [PubMed]
246. Yu, L.; Zhang, W.; Jiang, Y.; Guo, C. Gradient degradable nerve guidance conduit with multilayer structure prepared by electrospinning. *Mater. Lett.* **2020**, *276*, 128238. [CrossRef]
247. Hanumantharao, S.N.; Alinezhadbalalami, N.; Kannan, S.; Friske, M.; Rao, S. Electrospun acellular scaffolds for mimicking the natural anisotropy of the extracellular matrix. *RSC Adv.* **2019**, *9*, 40190–40195. [CrossRef]
248. Roshanbinfar, K.; Vogt, L.; Ruther, F.; Roether, J.A.; Boccaccini, A.R.; Engel, F.B. Nanofibrous Composite with Tailorable Electrical and Mechanical Properties for Cardiac Tissue Engineering. *Adv. Funct. Mater.* **2020**, *30*, 1908612. [CrossRef]
249. Roshanbinfar, K.; Vogt, L.; Ruther, F.; Roether, J.A.; Boccaccini, A.R.; Engel, F.B. Developing cellular therapies for retinal degenerative diseases. *Investig. Ophthalmol. Vis. Sci.* **2014**, *55*, 1191–1202.
250. Van Gelder, R.N.; Chiang, M.F.; Dyer, M.A.; Greenwell, T.N.; Levin, L.A.; Wong, R.O.; Svendsen, C.N. Regenerative and restorative medicine for eye disease. *Nat. Med.* **2022**, *28*, 1149–1156. [CrossRef]

251. Hotaling, N.A.; Khristov, V.; Wan, Q.; Sharma, R.; Jha, B.S.; Lotfi, M.; Maminishkis, A.; Simon, C.; Bharti, K. Nanofiber Scaffold-Based Tissue-Engineered Retinal Pigment Epithelium to Treat Degenerative Eye Diseases. *J. Ocul. Pharmacol. Ther.* **2016**, *32*, 272–285. [CrossRef]
252. Treharne, A.J.; Thomson, H.A.; Grossel, M.C.; Lotery, A.J. Developing methacrylate-based copolymers as an artificial Bruch's membrane substitute. *J. Biomed. Mater. Res. A* **2012**, *100*, 2358–2364. [CrossRef] [PubMed]
253. Warnke, P.H.; Alamein, M.; Skabo, S.; Stephens, S.; Bourke, R.; Heiner, P.; Liu, Q. Primordium of an artificial Bruch's membrane made of nanofibers for engineering of retinal pigment epithelium cell monolayers. *Acta Biomater.* **2013**, *9*, 9414–9422. [CrossRef] [PubMed]
254. Xiang, P.; Wu, K.C.; Zhu, Y.; Xiang, L.; Li, C.; Chen, D.L.; Chen, F.; Xu, G.; Wang, A.; Li, M.; et al. A novel Bruch's membrane-mimetic electrospun substrate scaffold for human retinal pigment epithelium cells. *Biomaterials* **2014**, *35*, 9777–9788. [CrossRef] [PubMed]
255. Sorkio, A.; Porter, P.J.; Juuti-Uusitalo, K.; Meenan, B.J.; Skottman, H.; Burke, G.A. Surface Modified Biodegradable Electrospun Membranes as a Carrier for Human Embryonic Stem Cell-Derived Retinal Pigment Epithelial Cells. *Tissue Eng. Part A* **2015**, *21*, 2301–2314. [CrossRef]
256. Komez, A.; Baran, E.T.; Erdem, U.; Hasirci, N.; Hasirci, V. Construction of a patterned hydrogel-fibrous mat bilayer structure to mimic choroid and Bruch's membrane layers of retina. *J. Biomed. Mater. Res. A* **2016**, *104*, 2166–2177. [CrossRef] [PubMed]
257. Phelan, M.A.; Kruczek, K.; Wilson, J.P.; Brooks, M.J.; Drinnan, C.T.; Regent, F.; Gerstenhaber, J.A.; Swaroop, A.; Lelkes, P.I.; Li, T. Soy Protein Nanofiber Scaffolds for Uniform Maturation of Human Induced Pluripotent Stem Cell-Derived Retinal Pigment Epithelium. *Tissue Eng. Part C Methods* **2020**, *26*, 433–446. [CrossRef]
258. Zeng, Z.; Lam, P.T.; Robinson, M.L.; Del Rio-Tsonis, K.; Saul, J.M. Design and Characterization of Biomimetic Kerateine Aerogel-Electrospun Polycaprolactone Scaffolds for Retinal Cell Culture. *Ann. Biomed. Eng.* **2021**, *49*, 1633–1644. [CrossRef]
259. Liu, Z.; Yu, N.; Holz, F.G.; Yang, F.; Stanzel, B.V. Enhancement of retinal pigment epithelial culture characteristics and subretinal space tolerance of scaffolds with 200 nm fiber topography. *Biomaterials* **2014**, *35*, 2837–2850. [CrossRef]
260. Sharma, R.; Khristov, V.; Rising, A.; Jha, B.S.; Dejene, R.; Hotaling, N.; Li, Y.; Stoddard, J.; Stankewicz, C.; Wan, Q.; et al. Clinical-grade stem cell–derived retinal pigment epithelium patch rescues retinal degeneration in rodents and pigs. *Sci. Transl. Med.* **2019**, *11*, eaat5580. [CrossRef]